This is a preprint of: "Phase portraits of separable Hamiltonian systems", Antoni Guillamon, Chara Pantazi, *Nonlinear Anal.*, vol. 74, 4012–4035, 2011.
DOI: [10.1016/j.na.2011.03.030]

Phase portraits of separable Hamiltonian systems*

Antoni Guillamon and Chara Pantazi
Dept. de Matemàtica Aplicada I,
Universitat Politècnica de Catalunya,
Dr. Marañón, 44-50, 08028, Barcelona, Catalonia, Spain.
Tel. number: (34) 934010904; FAX number: (34) 934011713
antoni.guillamon@upc.edu, chara.pantazi@upc.edu

April 5, 2011

Abstract

We study a generalization of potential Hamiltonian systems ($H(x,y) = y^2 + F(x)$) with one degree of freedom; namely, those with Hamiltonian functions of type $H(x,y) = F(x) + G(y)$, which will denoted by X_H. We present an algorithm to obtain the phase portrait (including the behaviour at infinity) of X_H when F and G are arbitrary polynomials. Indeed, from the graphs of the one-variable functions F and G, we are able to give the full description on the Poincaré disk, therefore extending the well-known method to obtain the phase portrait of potential systems in the finite plane. The fact that the phase portraits can be fully described in terms of the two one-variable real functions F and G allows, as well, a complete study of the bifurcation diagrams in complete families of vector fields. The algorithm can be applied to study separable Hamiltonian systems with one degree of freedom, which include a vast amount of examples in physical applications.

1 Introduction

Hamiltonian systems are ubiquitous in mathematical physics, specially in mechanics, but also in control engineering, biology and other fields. The goals in the study of Hamiltonian systems are diverse, according to the dimension (number of degrees of freedom) and the complexity of the Hamiltonian function H. In this paper, we deal with a relatively simple family of Hamiltonian systems (low dimensional and polynomial) but, in compensation, we are able to give an algorithm to plot the phase portrait including the behaviour at infinity, that is, to provide the full qualitative description of the associated dynamics. In particular, the algorithm allows the study of families of vector fields and their bifurcations in a rather simple way. Our target are the Hamiltonian systems

*Both authors are partially supported by the MICINN/FEDER grant MTM2009-06973 (DACOBIAN) and Generalitat de Catalunya CUR-DIUE grant number 2009SGR-859. Ch.P. is also supported by the MEC/FEDER grant MTM2008-03437.

with one-degree of freedom and separated variables, which energy function writes as:

$$H(x, y) = F(x) + G(y), \tag{1}$$

where x represents the phase, usually called q in the literature, and y the momentum, usually called p.

The main reason for the choice of this family is the balance between applicability and feasibility: on one hand, there is a vast literature on separable Hamiltonian systems and, on the other hand, there are no general algorithms to systematically study them except for the case $G(y) = y^2/2$. Thus, the results presented here can be potentially applied to relevant physical systems (see next paragraph), by means of a systematic procedure to obtain the full qualitative description of the orbits.

One can find examples of Hamiltonian systems of type (1) in classical textbooks, see for instance [**?**] and [**?**, Chap. II], but also more recent and specific examples can be found, for instance, in relativistic potentials or fluid kinetics. In the context of relativistic mechanics, [**?**], for instance, study constant period oscillators in the family $H(p, q) = \sqrt{p^2\, c^2 + m^2\, c^4} - m\, c^2 + V(q)$, where p is the momentum and c the speed of light. In fluid kinetics, Stommel, see [**?**], used a non-trivial Hamiltonian system with separable variables with the goal of modeling the behaviour of particles through a fluid flow field without inertia. When adding a small inertia, the system is no longer Hamiltonian but the information about the phase portrait of the Stommel's Hamiltonian is important (see for instance [**?**]).

Apart from direct examples of type (1), there has been a wide interest in the literature to investigate whether a general Hamiltonian system can be brought into separated variables, see for instance [**?**] in the context of Yang-Mills theories or, in control engineering, [**?**] and the references therein. It is obvious that such a reduction in a suitable set of variables facilitates the study of the Hamiltonian system; in particular, there also exists an extensive literature in numerical analysis concentrated on building up symplectic integration algorithms (thus maintaining the symplectic structure) devoted to separable Hamiltonian systems; representative examples can be found in [**?**], [**?**] or [**?**]. For instance, no explicit symplectic Runge-Kutta methods exist for general Hamiltonians which are not separable. This numerical approach to systems of type (1) makes more sense in higher dimensions; in this work, instead, we are concerned to give a complete topological description of Hamiltonians with separated variables and one degree of freedom. Thus, every one degree of freedom separable Hamiltonian system, once the canonical transformation has brought it into a separated Hamiltonian, may be a candidate to apply our method.

Beyond the applications exposed above, which demand a good knowledge of Hamiltonian systems of type (1), these Hamiltonians have also been thoroughly studied in the context of qualitative theory of differential equations. In general, the study of phase portraits of Hamiltonian systems is useful for the so-called *weakened* or *infinitesimal Hilbert 16th problem* that asks for the number of limit cycles that may appear when perturbing a polynomial Hamiltonian systems (see for instance [**?**]). For this purpose, it is important to know the number and distribution of centers, and the respective period annuli. Methods to track the orbits of the conservative system that remain closed after perturbation are then applied: Melnikov functions, averaging, singular geometric perturbations,... In the non perturbed (Hamiltonian) dynamics it is also relevant the classification of centres (bounded versus non-bounded, global versus non-global,...) for their transcendence to give properties of the period function associated to them, see for instance [**?**] for a "classical" reference. Thus, the possibility of obtaining the phase portraits of a certain family of vector fields provides

a direct way to control all the possible types of centres appearing in such a family. Recently, the knowledge of the period annuli has been also combined with new techniques to study the period function associated to centres, see [**?**] or [**?**] as representative, [**?**] for the first applications to the family (1) and [**?**] for a general formula for the period function and also a number of applications inside the family (1).

Besides the relevance of the phase portraits of type (1) both for physical/engineering applications and to important problems in dynamical systems, from a more constructive point of view, it is worthy noting that algorithms to plot general classes of Hamiltonian vector fields are not easy to obtain. For instance, papers in the recent literature are devoted to obtain phase portraits of families of low degree polynomial vector fields having degree 2 rational first integrals, see for instance [**?**] or [**?**].

The best known and more classical example is the algorithm to plot the finite phase portrait of potential systems with one degree of freedom. The clue to be able to topologically classify this type of Hamiltonian systems is, obviously, the simplicity of its energy function, $H(x, y) = y^2/2 + F(x)$, with $F \in C^1(\mathbb{R})$ (see Fig. 1).

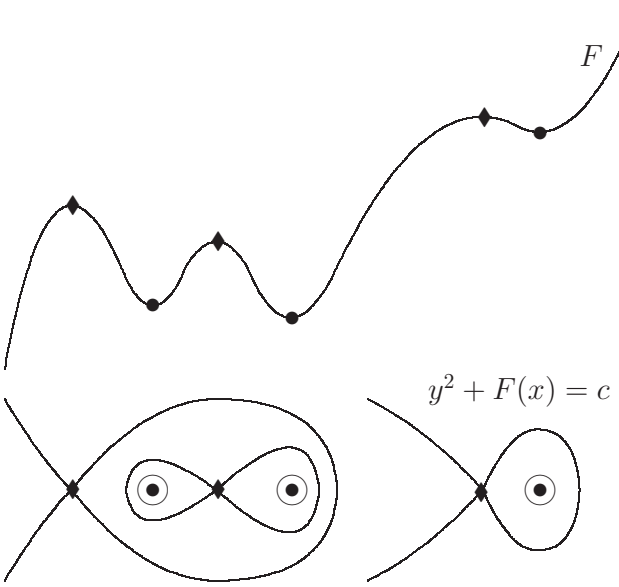

Figure 1: Finite representation of the phase portrait of a potential system; minima of F coincide with centre points ($\bullet$) while maxima coincide with saddle points ($\blacklozenge$).

In potential systems, the fact that H "depends" basically on $F(x)$ allows to relate the phase portrait of $\{\dot{x} = -H_y(x, y),\ \dot{y} = H_x(x, y)\}$ with the graph of the one-variable function $F(x)$. This kind of reduction was also explored in [**?**] for Hamiltonian systems of type $\mathcal{G}(r, \theta) = r^2/2 + r^{n+1}\, g(\theta)$, in which the detailed knowledge of g provides the full information about the phase portrait of $X_{\mathcal{G}}$ (along the paper, we use the notation X_E to denote the Hamiltonian vector field obtained from the Hamiltonian function E, with E defined on some subset of $\mathbb{R}^2$).

In this work, we extend this type of results by giving a general algorithm to obtain the global phase portrait Hamiltonian systems of type (1). By "global phase portrait" we understand the

phase portrait including the behaviour at infinity. Observe that (1) can be written as:

$$\dot{x} = -G'(y), \qquad \dot{y} = F'(x), \tag{2}$$

where the dot denotes the derivative with respect to time, and the prime denotes the derivative with respect to the phase variables. We will refer to this vector field as X_H. Our description includes the classical classification of finite singular points of smooth potential systems. The use of the Poincaré compactification to study the infinity forces us to require F and G to be polynomials; however, most of the results (except those referring behaviour at infinity) are also true for the non-polynomial case.

We want to stress the fact that we perform this study with F and G being arbitrary polynomials. On one hand, it adds difficulty to the task of obtaining a complete algorithm that takes into account all the combinations among the energy levels of the separatrices but, on the other hand, it provides a way to study bifurcation diagrams of subfamilies of (2). The key point is the possibility of reducing the study of the phase portrait to the study of a short number of one-variable real functions; that is, determining the phase portrait of a vector field from the graphs of F and G; Fig. 2 illustrates this fact. This advantage is exemplified in this paper throughout some families of vector fields that have not been studied previously; the technique can be extended to any subfamily of Hamiltonian vector fields of type (2). It is not our goal here to be exhaustive by counting all the possible configurations of the relative positions of maxima and minima of F and G. This could be a challenging problem but, apart from being a cumbersome combinatorial task, the possible results would not shed more light to the qualitative description of the phase portraits.

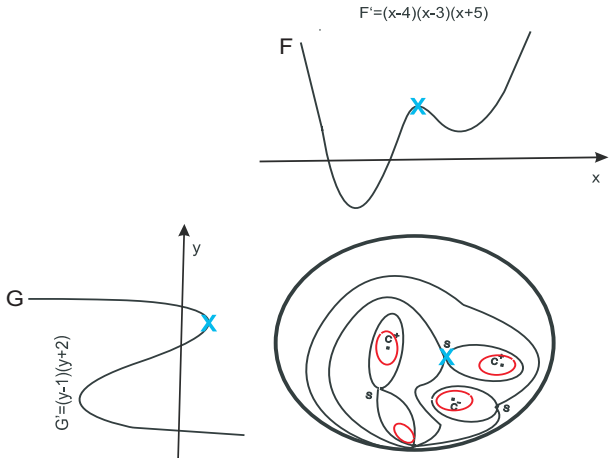

Figure 2: Example of how the geometry of F and G determines the phase portrait.

The rest of the paper is divided in other four sections: we start by presenting the most practical and concise version of the general algorithm in Section 2. For the sake of clearness, details and proofs necessary to understand the paper at a deeper level are sent to Section 5. In between, Sections 3 and 4 contain examples of global phase portraits of representative vector fields (Section 3) and examples of bifurcations of families of vector fields (4) obtained from the algorithm just from the knowledge of the bifurcations of one-variable families of functions.

2 Algorithm

We present the algorithm to plot the phase portrait of systems of type (2) at three levels of description: first, we outline the general overview of the algorithm (in this section); second, we sketch out the basic steps to perform it (in this section); and, third, we detailed the proofs of the results used in the second level (see Section 5). This organization allows the reader to directly apply the algorithm without needing to dive into technical details.

2.1 Algorithm: major steps

At a first level of description, these are the main steps to get the global phase portrait:

(a) Determine all the finite singular points, classify them topologically and order them according to the energy levels, using results given in Subsection 2.2.

(b.1) Localize and classify the infinite singular points, using Table 1 in Subsection 2.3.

(b.2) Plot the separatrices connecting infinity with the finite singular points defined in Definition 5, applying Proposition 6 (see Subsection 2.4.1).

(c.1) Surround all finite centres by their proximal separatrices following Proposition 8 in Subsection 2.4.2.

(c.2) Identify the bounded extended graphics created in step (c.1) and surround them by separatrices according to Proposition 11 in Subsection 2.4.2.

Connect all the remaining separatrices by allowing extended graphics containing singular points at infinity, again according to Proposition 11.

The following subsections are devoted, respectively, to steps (a), (b) and (c); they deal with finite singular points, singular points at infinity and organization of separatrices, respectively.

2.2 Finite singular points

Without loss of generality, we will assume that the origin is a singular point of system (2), which implies that $F'(0) = G'(0) = 0$. To fix notation, we write:

$$F'(x) = a_n\, x^n + \ldots + a_1\, x, \quad a_n \neq 0; \quad G'(y) = b_m\, y^m + \ldots + b_1\, y, \quad b_m \neq 0. \tag{3}$$

Hence, system (2) is equivalent to:

$$\left\{ \begin{array}{lll} \dot{x} & = -G'(y) & = -(b_m\, y^m + \ldots + b_1\, y), \\ \dot{y} & = F'(x) & = a_n\, x^n + \ldots + a_1\, x, \end{array} \right.$$

with $a_n \neq 0$ and $b_m \neq 0$.

We will consider only the case $n \geq m$. It is obvious that the case $m > n$ can be deduced from it by interchanging the role of the state variables.

For the hyperbolic singular points (which in this case are the saddles coming from simple zeroes of F' and G'), it is obvious that Hartman's theorem gives a direct classification. On the other hand, singular points of (2) with pure imaginary eigenvalues are centres. However, there are still other singular points of system (2) which are not hyperbolic or linear centres and they require *ad hoc* arguments to be classified. Next result gives the topological description of any finite singular point.

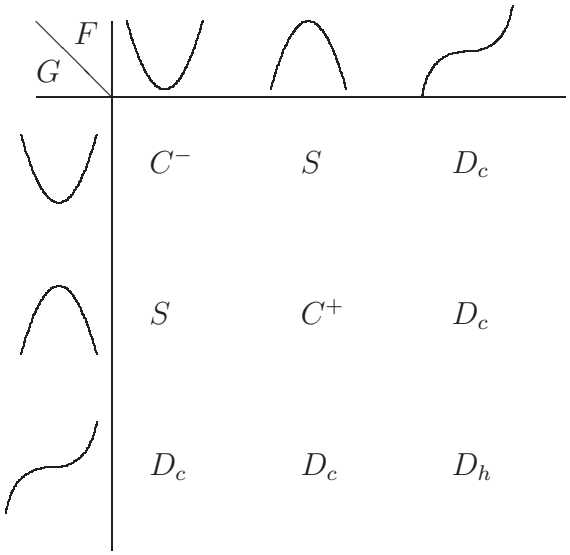

Figure 3: Different types of finite singular points, see Proposition 1, according to the topological nature of F and G on their critical values. Here, S stands for saddle, C for centre and D for degenerate point, either cusp (D_c) or union of two hyperbolic sectors (D_h).

Proposition 1 (Finite singular points)**.** *Let $P = (x_0, y_0)$ be a finite singular point of system (2). Then, $F'(x_0) = G'(y_0) = 0$ and*

(a) P is a saddle (denoted by (S)) if and only if F has a maximum (resp., a minimum) at x_0 and G has a minimum (resp., a maximum) at y_0.

(b) P is a centre point (C) if and only if one of the two following conditions holds:

(b.1) F has a maximum at x_0 and G has a maximum at y_0 (denoted by (C^-));

(b.2) F has a minimum at x_0 and G has a minimum at y_0 (denoted by (C^+)).

(c) P is a cusp point (D_c) if and only if one of the two following conditions holds:

- *F has an inflection point at x_0 and G has a maximum or a minimum at y_0;*
- *G has an inflection point at y_0 and F has a maximum or a minimum at x_0.*

(d) P is a singular point formed by the union of two hyperbolic sectors (D_h) if and only if F has an inflection point at x_0 and G has an inflection point at y_0.

Proposition 1 covers all the possible cases; so, we can only have saddles, centres, cusps or union of two hyperbolic sectors. Observe that both the saddles in statement (a) and the centres in statement (b) can be degenerate; that is, the classification is based on the topological nature of the functions F and G rather than their algebraic nature.

Figure 3 illustrates in a graphical way how the different types of singular points arise from the topological nature of F and G on their critical values.

2.3 Singular points at infinity

In order to study the behaviour of system (2) near infinity we use the Poincaré compactification (see for instance [**?**]). We denote by $\{X_1, X_2, X_3\}$ the coordinates on the sphere $\mathbb{S}^2$, being $X_3 = 0$ its equator. We will consider the restriction of the extended/compactified vector field $\overline{X_H}$ to different charts: (U_i, ψ_i), defined on $\{X_i > 0\}$, and (V_i, ϕ_i), defined on $\{X_i < 0\}$, for $i = 1, 2, 3$. Since opposite charts (U_i, ψ_i) and (V_i, ϕ_i) have the same phase portraits (with time-reversals when n is odd), we will mainly focus on the description of the vector field on the (U_i, ψ_i) charts. On the other hand, we will represent the phase portraits on the Poincaré disk (projection of $\overline{X_H}$ for $X_3 \geq 0$ on $\mathbb{D}$; indeed, chart (U_3, ψ_3) plus $\{X_3 = 0\}$). See Section 5.3 for the details concerning the compactification and the expression of $\overline{X_H}$ on each chart.

Lemma 2. *Consider system (2) with $n \geq m$. Then,*

1. *If $n > m$, the vector field $\overline{X_H}$ has exactly 2 singular points on the equator of the Poincaré sphere: the origin of the (U_2, ψ_2) (denoted by q^+_{inf}) chart and the origin of the (V_2, ϕ_2) chart (denoted by q^-_{inf}), see Fig. 4 (left).*

2. *If $n = m$, the singular points at infinity are given by: ${z_1}^{n+1} = -\dfrac{a_n}{b_n}$ on the (U_1, ψ_1) chart and ${z_1}^{n+1} = -\dfrac{b_n}{a_n}$ on the (U_2, ψ_2) chart. More precisely,*

   (a) *if $n = m$ is odd and $b_n/a_n < 0$, we have 2 singular points on all the charts: (U_1, ψ_1), (V_1, ϕ_1), (U_2, ψ_2) and (V_2, ϕ_2). However, the 4 singular points on $(U_1, \psi_1) \cup (V_1, \phi_1)$ coincide (on the Poincaré sphere) with the 4 singular points on $(U_2, \psi_2) \cup (V_2, \phi_2)$, see Fig. 4 (center);*

   (b) *if $n = m$ is odd and $b_n/a_n > 0$, we have no singular points at infinity, see Fig. 4 (right);*

   (c) *if $n = m$ is even, we have 2 singular points at infinity (denoted by $\tilde{q}^+_{inf}$ and $\tilde{q}^-_{inf}$), diametrally opposed, but different from q^+_{inf} and q^-_{inf}. The points $\tilde{q}^+_{inf}$ and $\tilde{q}^-_{inf}$ tend to q^+_{inf} and q^-_{inf}, resp., when $b_m \to 0$.*

In some steps of the algorithm it is useful to "dissect" the dynamics into "minimal" units. In fact, given the separability of variables in $H(x, y)$, the finite singular points are arranged in a reticular way thus defining special cells whose corners are the finite singular points, see Fig. 5.

Definition 3. *Let us suppose that $F'(x)$ vanishes at x_i for $i = 1, \ldots, r$, and $G'(y)$ vanishes at y_j for $j = 1, \ldots, s$. In the reticular division of the plane, we distinguish the following types of* cells *(see also Fig. 5):*

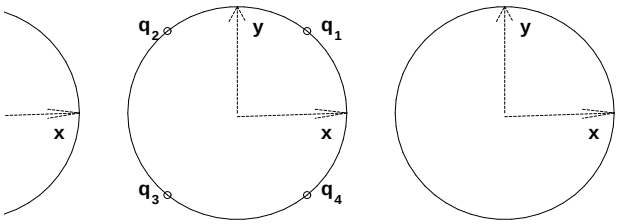

Figure 4: Singular points at infinity on the Poincaré disk. For $n > m$, the point q^+_{inf} is the origin of the chart (U_2, ψ_2) whereas q^-_{inf} is the origin of the chart (V_2, ϕ_2), see (a). When $n = m$, there can exist either four (q_1, q_2, q_3, q_4), see (b), two (a pair $\tilde{q}^+_{inf}, \tilde{q}^-_{inf}$, see (c), or q_2, q_4) or zero singular points. The boundary of the disk ($X_3 = 0$) is always invariant. All the global phase portraits will be shown on the Poincaré disk. We leave the notation (x, y) to see the directions of the original variables.

- **Rectangular cells**. *Given a pair (i, j), with $i < r$ and $j < s$, we denote by $\mathbf{R_{ij}}$ the finite rectangle of the plane whose vertices are the points (x_i, y_j), (x_i, y_{j+1}), (x_{i+1}, y_{j+1}) and (x_{i+1}, y_j).*
- **Corner cells** *are the unbounded cells whose borders are the union of the half-lines $L_x := \{ x \geq (\leq) x_\sigma, y = y_{\sigma'}\}$ and $L_y := \{x = x_\sigma,\ y \geq (\leq) y_{\sigma'}\}$ with the singular point $\{(x_\sigma, y_{\sigma'})\}$, where $(\sigma, \sigma') \in \{(1,1), (1,s), (r,1), (r,s)\}$. The sign $\leq$ in the definition of the borders applies when $\sigma = 1$ or $\sigma' = 1$, and the sign $\geq$ applies when $\sigma = r$ or $\sigma' = s$. We label each of the four corner cells as $\mathbf{Q}^{\sigma\sigma'}$ if in this cell we have that $(-1)^\sigma x > 0$ and $(-1)^{\sigma'} y > 0$.*
- **Semi-rectangular cells** *are unbounded cells that are not corner cells; that is, those having on its border two finite singular points of the form $\{(x_\sigma, y_{\sigma'})\}$, where $\sigma \in \{1, r\}$ and $\sigma' \in \{1, s\}$.*

In the absence of inflection points of F and G, the finite singular points alternate between saddles and centres (also alternating type C^+ and type C^- in each row/column). In fact, when we have a degenerate point (cusp or two hyperbolic sectors), we can run the algorithm just ignoring them and adding them at the end, so that we can assume (without loss of generality) that the finite singular points are either saddles or centres, see also Remark 12.

The study of the vector field on the corner cells gives enough information to classify the singular points at infinity. Their topological type basically depends on the parity of both functions F and G and the sign on the leading monomials. We have chosen here the shortest way to show this classification. There are, of course, analytical methods to analyse it (use of Hartman's Theorem plus blow-up techniques... with no *a priori* bounds!) or more topological ones taking advantage of index theory and additional reasonings, see Remark 15. The result is given in the next proposition and abridged in Table 1; the resulting types of singular points on the Poincaré sphere are displayed in Fig. 6.

Proposition 4. *Let us consider system (2) on the Poincaré disk, with the notation given in (3), and $n > m$. Then, according to the parities of n and m, and the sign of a_n and b_m, the singular points of (2) at infinity have the topological types defined in Table 1, with the following conventions:*

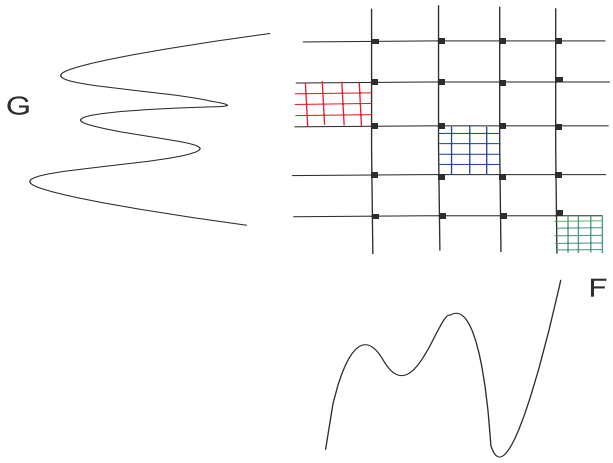

Figure 5: Different types of cells. Three cells highlighted; from left to right: semi-rectangular, rectangular and corner cell.

- *The symbol in the entry $\mathcal{Q}_{\sigma\sigma'}$ of $\mathcal{Q}$ (see Table 1) denotes whether the orbits of (2) in the corner cell $Q^{\sigma\sigma'}$ tend to $q_{inf}^{\sigma'}$ in forward (A) or backward (R) time, or leave the corner cell both in forward and backward time ($\emptyset$)*
- *The symbol in the entries of $\begin{pmatrix} q_{inf}^{+} \\ q_{inf}^{-} \end{pmatrix}$ denotes whether the corresponding singular point at infinity in the Poincaré disk presents an attracting nodal sector (N_A), a repelling nodal sector (N_R), a hyperbolic sector (H) or an elliptic sector (E).*
- *In the case $n = m$ the singular points with hyperbolic sectors disappear, whereas those with elliptic sectors split into two nodes. The stability of these nodes is determined by the corresponding Q matrix of Table 1.*

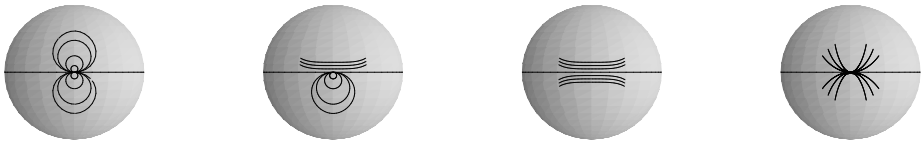

Figure 6: Possible topological types of singular points at infinity on the Poincaré sphere. On the Poincaré disk, only one of the two sectors is *visible*, depending on the parity of the vector field, see Table 1.

			n even		n odd	
m	a_n	b_m	$\mathcal{Q} = \begin{pmatrix} Q^{-+} & Q^{++} \\ Q^{--} & Q^{+-} \end{pmatrix}$	$\begin{pmatrix} q^+_{inf} \\ q^-_{inf} \end{pmatrix}$	$\mathcal{Q} = \begin{pmatrix} Q^{-+} & Q^{++} \\ Q^{--} & Q^{+-} \end{pmatrix}$	$\begin{pmatrix} q^+_{inf} \\ q^-_{inf} \end{pmatrix}$
even	$+$	$+$	$\begin{pmatrix} A & \emptyset \\ \emptyset & R \end{pmatrix}$	$\begin{pmatrix} N_A \\ N_R \end{pmatrix}$	$\begin{pmatrix} \emptyset & \emptyset \\ A & R \end{pmatrix}$	$\begin{pmatrix} H \\ E \end{pmatrix}$
even	$+$	$-$	$\begin{pmatrix} \emptyset & A \\ R & \emptyset \end{pmatrix}$	$\begin{pmatrix} N_A \\ N_R \end{pmatrix}$	$\begin{pmatrix} R & A \\ \emptyset & \emptyset \end{pmatrix}$	$\begin{pmatrix} E \\ H \end{pmatrix}$
even	$-$	$+$	$\begin{pmatrix} \emptyset & R \\ A & \emptyset \end{pmatrix}$	$\begin{pmatrix} N_R \\ N_A \end{pmatrix}$	$\begin{pmatrix} A & R \\ \emptyset & \emptyset \end{pmatrix}$	$\begin{pmatrix} E \\ H \end{pmatrix}$
even	$-$	$-$	$\begin{pmatrix} R & \emptyset \\ \emptyset & A \end{pmatrix}$	$\begin{pmatrix} N_R \\ N_A \end{pmatrix}$	$\begin{pmatrix} \emptyset & \emptyset \\ R & A \end{pmatrix}$	$\begin{pmatrix} H \\ E \end{pmatrix}$
odd	$+$	$+$	$\begin{pmatrix} A & \emptyset \\ R & \emptyset \end{pmatrix}$	$\begin{pmatrix} N_A \\ N_R \end{pmatrix}$	$\begin{pmatrix} \emptyset & \emptyset \\ \emptyset & \emptyset \end{pmatrix}$	$\begin{pmatrix} H \\ H \end{pmatrix}$
odd	$+$	$-$	$\begin{pmatrix} \emptyset & A \\ \emptyset & R \end{pmatrix}$	$\begin{pmatrix} N_A \\ N_R \end{pmatrix}$	$\begin{pmatrix} R & A \\ A & R \end{pmatrix}$	$\begin{pmatrix} E \\ E \end{pmatrix}$
odd	$-$	$+$	$\begin{pmatrix} R & \emptyset \\ A & \emptyset \end{pmatrix}$	$\begin{pmatrix} N_R \\ N_A \end{pmatrix}$	$\begin{pmatrix} A & R \\ R & A \end{pmatrix}$	$\begin{pmatrix} E \\ E \end{pmatrix}$
odd	$-$	$-$	$\begin{pmatrix} \emptyset & R \\ \emptyset & A \end{pmatrix}$	$\begin{pmatrix} N_R \\ N_A \end{pmatrix}$	$\begin{pmatrix} \emptyset & \emptyset \\ \emptyset & \emptyset \end{pmatrix}$	$\begin{pmatrix} H \\ H \end{pmatrix}$

Table 1: Singular points at infinity as a function of degrees and signs of F and G for $n > m$, see Proposition 4. Legend: A = attractor corner cell at infinity; R = repelling corner cell at infinity; $\emptyset$ = corner cell neither attracting nor repelling; N_A = stable node; N_R = unstable node; E = elliptic sector; H = hyperbolic sector. The labels $Q^{\sigma\sigma'}$ refer to the four corner cells (see definition in the text); q^-_{inf} and q^+_{inf} are the two singular points at infinity.

2.4 Organisation of separatrices

2.4.1 Special saddle points and separatrices: connecting finite points to infinity

One of the crucial steps to obtain the global phase portrait is to determine which separatrices connect with singular points at infinity. For this purpose, we need to distinguish special maxima and minima of functions F and G, which will be specially interesting in the case that $S^* = (x^*, y^*)$ is a saddle. Let us, then, introduce some vocabulary.

Definition 5. *Given a real-valued continuous function F, we say that:*

- *x^* satisfies the* property *f_l (resp., $\mathcal{F}_l$) if $F(x^*)$ is a minimum (resp., maximum) of F and $F(x) > F(x^*)$ (resp., $F(x) < F(x^*)$) for each $x < x^*$.*
- *x^* satisfies the* property *f_r (resp., $\mathcal{F}_r$) if $F(x^*)$ is a minimum (resp., maximum) of F and $F(x^*) < F(x)$ (resp., $F(x^*) > F(x)$) for each $x > x^*$.*

The same rules are used to define g_l, $\mathcal{G}_l$, g_r and $\mathcal{G}_r$.

A saddle point $S^* = (x^*, y^*)$ will be said to be of type (A, B) *if x^* satisfies property A ($A \in \{f_l, f_r, \mathcal{F}_l, \mathcal{F}_r\}$) and y^* satisfies property B ($B \in \{g_l, g_r, \mathcal{G}_l, \mathcal{G}_r\}$). Observe that a saddle is either not classifiable with this criterium or is of one of the following types: $(f_l, \mathcal{G}_r)$, $(f_l, \mathcal{G}_l)$, $(f_r, \mathcal{G}_r)$, $(f_r, \mathcal{G}_l)$, $(\mathcal{F}_l, g_r)$, $(\mathcal{F}_l, g_l)$, $(\mathcal{F}_r, g_r)$, $(\mathcal{F}_r, g_l)$.*

*The four separatrices of any saddle are organized in a topographical way so that we can distinguish them according to the cell through which they reach the saddle. Accordingly, we define the ll-*separatrix *of S^* (respectively, lr-, rl- and rr-) to be the left-down separatrix (respectively, left-up, right-down, right-up) of S^*.*

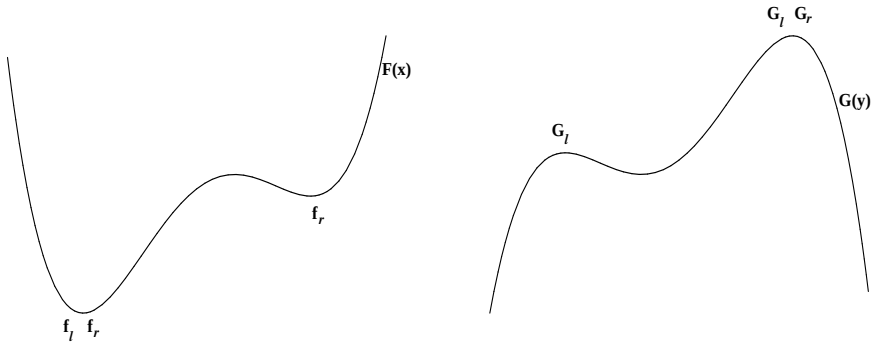

Figure 7: Some properties of the critical points of F and G, see Definition 5.

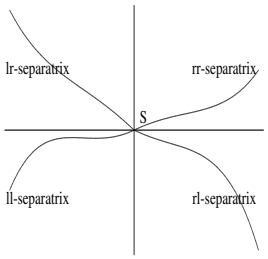

Figure 8: Graphical representation of the four types of separatrices.

When these properties apply to our functions F and G, we can distinguish special landmarks of the phase portrait of system (2):

Proposition 6. *Consider a finite saddle point $S^* = (x^*, y^*)$ of system (2). Suppose that S^* is of type $(f_l, \mathcal{G}_l)$ or $(\mathcal{F}_l, g_l)$ (respectively, $(\mathcal{F}_l, g_r)$ or $(f_l, \mathcal{G}_r)$; $(\mathcal{F}_r, g_l)$ or $(f_r, \mathcal{G}_l)$; $(f_r, \mathcal{G}_r)$ or $(\mathcal{F}_r, g_r)$). Then,*

1. *when $n > m$, its ll- (resp., lr-; rl-; rr-) separatrix tends to or comes from q^-_{inf} (resp., q^+_{inf}, q^-_{inf}, q^+_{inf}).*
2. *when $n = m$ is even, its ll- (resp., lr-; rl-; rr-) separatrix tends to or comes from $\tilde{q}^-_{inf}$ (resp., $\tilde{q}^+_{inf}$, $\tilde{q}^-_{inf}$, $\tilde{q}^+_{inf}$).*

3. *when $n = m$ is odd and $b_n/a_n < 0$, its ll- (resp., lr-; rl-; rr-) separatrices tend to or come from q_3 (resp., q_2, q_4, q_1).*

Observe that Proposition 6 both claims the connection of special finite saddles with the singular points at infinity and states the stability character of these separatrices with respect to the singular points. A direct consequence is the following result.

Corollary 7. *The elliptic sectors at infinity appear only for $n > m$ and can be formed in the following ways:*

1. *The point q^+_{inf} has an elliptic sector if and only if there exist finite saddles S^* both of type $(f_r, \mathcal{G}_r)$ and $(f_l, \mathcal{G}_r)$ (or $(\mathcal{F}_r, g_r)$ and $(\mathcal{F}_l, g_r)$).*
2. *The point q^-_{inf} has an elliptic sector if and only if there exist finite saddles S^* both of type $(f_r, \mathcal{G}_l)$ and $(f_l, \mathcal{G}_l)$ (or $(\mathcal{F}_r, g_l)$ and $(\mathcal{F}_l, g_l)$).*

2.4.2 Structure of the set of separatrices

In Proposition 6, we have already analyzed those separatrices for which we can ensure to reach a specific singular point at infinity. Some other separatrices will reach infinity as well, but no general rule can be stated at this point. To make it clearer, it is useful to study the organization of the separatrices in an increasing order of complexity. In general, they organize themselves to embrace the different centres or more complex structures of the phase portrait.

The first step is to identify simple rules to surround the finite centre type points.

Proposition 8. *Let $C = (x_i, y_j)$, for some $1 \le i \le r$ and $1 \le j \le s$, be a singular point of centre type, S a finite saddle point, and $\mathcal{N}_C := \{(x_{i'}, y_{j'}) : |i' - i| + |j - j'| = 1\}$ the set of neighbouring points of C. Then,*

a) if C is of type C^+, it is embraced by the proximal separatrices of the neighbouring saddle S^* (that is, $S^* \in \mathcal{N}_C$) which energy level satisfies

$$H(S^*) = \min_{S \in \mathcal{N}_C} \{H(S) : H(S) > H(C)\}.$$

b) if C is of type C^-, it is embraced by the proximal separatrices of the neighbouring saddle S^* which energy level satisfies

$$H(S^*) = \max_{S \in \mathcal{N}_C} \{H(S) : H(S) < H(C)\}.$$

c) the separatrices of S can only embrace one type of centre, either C^+ or C^-.

In different words, C^+ has to be embraced by saddles with higher energy values and C^- has to be embraced by saddles with lower energy values.

From Proposition 8, it is easy to see that neighbouring centres and saddles can form more complex bounded structures, the simplest example being the union of a saddle point and its four

separatrices forming two homoclinic loops embracing two different centres, see Fig. 9(a). We could eventually have several saddles with the same energy level surrounding several centres as in Figure 9(b). We name these structures by $\mathcal{P}_0$ and remark their basic properties.

Remark 9. *Let $\mathcal{P}_0$ be a set formed by bounded period annuli of centres surrounded by separatrices of the same energy level. Then, the set $\mathcal{P}_0$ inherits the character of the embraced centres; that is, it can be classified into class $\mathcal{P}_0^+$ or $\mathcal{P}_0^-$ according to the preference of being embraced by higher or lower energy levels.*

Having defined these basic structures, we generalize them in the next definition.

Definition 10. *We call* **extended graphic** *to a subset $\mathcal{P}$ of the phase portrait in the Poincaré disk whose boundary is formed by singular points of system (2) and their separatrices. As for the centres, we define the set of the neighbouring points as $\mathcal{N}_\mathcal{P} = \bigcup_{C\in\mathcal{P}} \mathcal{N}_C \bigcap \mathcal{P}^c$, where $\mathcal{P}^c$ is the complement of $\mathcal{P}$ in the set of singular points.*

In fact, extended graphics $\mathcal{P}$ are nests of homoclinic and heteroclinic loops starting from type $\mathcal{P}_0$ structures, as it can be seen in Figure 9(c). Note that this definition allows the separatrices to reach singular points at infinity (see Fig. 10). Observe also that the boundary of an extended graphic can be embraced by separatrices of other saddles. Thus, starting from the simplest ones (type $\mathcal{P}_0$), extended graphics are formed hierarchically and also inherit the preference to higher ($\mathcal{P}^+$) or lower ($\mathcal{P}^-$) energy levels. Instances of these two facts can be found, for example, Fig. 9(c) or Fig. 12.

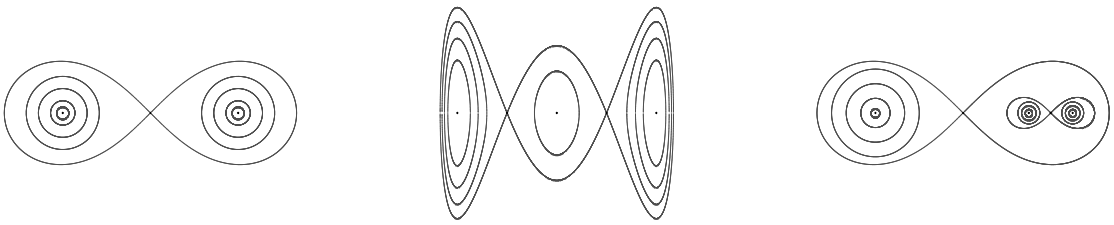

(a) (b) (c)

Figure 9: Examples of bounded extended graphics; cases (a) and (b) correspond to type $\mathcal{P}_0$.

Taking into account the previous definitions we state the following result.

Proposition 11. *Let $\mathcal{P}$ be an extended graphic. Then,*

a) if $\mathcal{P}$ is of type $\mathcal{P}^+$, it is embraced by the proximal separatrices of the neighbouring saddle S^* ($S^* \in \mathcal{N}_\mathcal{P}$) which energy level satisfies

$$H(S^*) = \min_{S\in\mathcal{N}_\mathcal{P}} \{H(S) : H(S) > H(\mathcal{P})\}.$$

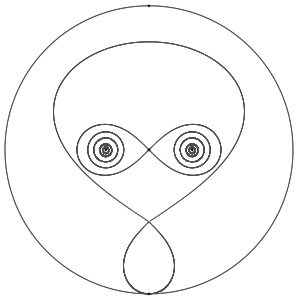

Figure 10: Extended graphic on the Poincaré disk that reaches a point at infinity.

b) if $\mathcal{P}$ is of type $\mathcal{P}^-$, it is embraced by the proximal separatrices of the neighbouring saddle S^* ($S^* \in \mathcal{N}_{\mathcal{P}}$) which energy level satisfies

$$H(S^*) = \max_{S \in \mathcal{N}_{\mathcal{P}}} \{H(S) : H(S) < H(\mathcal{P})\}.$$

c) the separatrices of S can only embrace one type of extended graphic, either $\mathcal{P}^+$ or $\mathcal{P}^-$.

3 Examples: single phase portraits

In order to illustrate the whole procedure we build up the global phase portrait of four representative cases in the following examples. Afterwards, in Section 4, we will examine how the algorithm can be applied to study bifurcations of families of vector fields.

Example 1. *Consider any system of type*

$$\begin{cases} x' &= -y(y - y_1), \\ y' &= x(x - x_1)(x - x_2), \end{cases} \tag{4}$$

with $0 < x_2 < -x_1$ and the energy distribution of finite singular points given in Fig. 11 (right panel).

Under these conditions, the functions $F(x) = \int x(x - x_1)(x - x_2)\,dx$ and $G(y) = \int y(y - y_1)\,dy$ have the qualitative portraits shown in Fig. 11 (all the comments in the example can be followed in this figure).

We label the critical points according to their energy levels. For instance, the upper-left point in the phase portrait comes from the first zero of F', that is $x = x_1$ and the highest zero of G', that is $y = 0$. Observe that: (1) it is a centre since it comes from two minima, so the label "C^+"; (2) it is the finite singular with the lowest energy level, so the subindex "1".

Being S_2 the neighbouring saddle of C_1 with closest energy level, their upper separatrices must embrace C_1. Similarly, S_4 embraces C_3 and S_5 embraces C_6.

Since $n = 3$ is odd, $m = 2$ is even and a_n, $b_n > 0$, from Proposition 4, we have $\mathcal{Q} = \begin{pmatrix} \emptyset & \emptyset \\ A & R \end{pmatrix}$ *and so q^+_{inf} has a hyperbolic sector whereas q^-_{inf} has an elliptic sector.*

Observe also that the saddle S_2 satisfies the properties f_r, f_l and $\mathcal{G}_l$; from Proposition 6, both lower separatrices of the saddle S_2 tend to q^-_{inf} (elliptic sector) and so the four separatrices of S_2 together with q^-_{inf} form an extended graphic, which we denote by S_2^{+1}. Then, the saddle S_4 becomes the neighbouring singular point of S_2^+ with closest energy and so, it embraces the extended graphic S_2^+ forming a new extended graphic S_4^+. At the end, the saddle S_5 embraces S_4^+ (alternatively, one could also use that S_5 satisfies f_r and $\mathcal{G}_l$, so that its $rl-$separatrix must connect to q^-_{inf}).

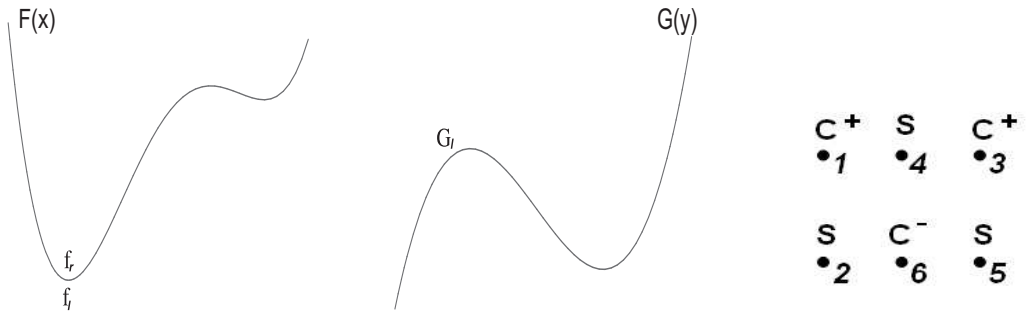

Figure 11: The graphs of the functions F and G of system (5) together with the distribution, labelling and energy ordering of the finite singular points.

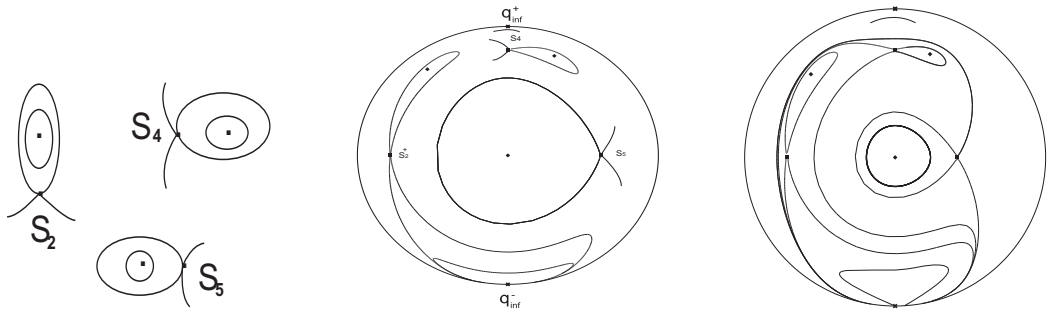

Figure 12: The global phase portrait of system (4) (right panel) and the last two steps, (c.1) and (c.2), of the algorithm.

Example 2. *We consider a more complex example, to be able to illustrate most of the features studied along the paper:*

$$\begin{cases} x' &= -y(y-4)(y-9), \\ y' &= x(x-1)(x-3)(x-6)(x^2+1). \end{cases} \tag{5}$$

It is a specific example, but any other polynomial vector field having F and G topologically equivalent to those of (4), with the same relative positions of the critical points of both functions, would have the same phase portrait.

[1] Although in the definition we denote by $\mathcal{P}$ the extended graphics, we prefer to use the notation S_j^+ to keep track of the saddle that provides the energy level of $\mathcal{P}$.

The comments of this example are based on the panels of Fig. 13. We will not be exhaustive since there are many repetitive operations; instead, we are going to highlight salient details. The first three panels are straightforward, as in Example 1. Departing from the fourth panel, in which neighbouring saddles embrace the centres following Section 2.4.2, we observe that saddles S_{10} and S_3 become S_{10}^- and S_3^+, respectively (see Proposition 8) since their four separatrices remain all bounded and form two heteroclinic loops around centres. In the fifth panel, the saddles S_6 and S_9 embrace, respectively, the extended graphics S_3^+ and S_{10}^+. Since m is odd and n is even, from Proposition 4 we note that does not appear elliptic sectors at infinity. Moreover, since $a_n > 0$ and $b_n > 0$ we have that $\mathcal{Q} = \begin{pmatrix} A & \emptyset \\ R & \emptyset \end{pmatrix}$ and therefore $\begin{pmatrix} q_{inf}^+ \\ q_{inf}^- \end{pmatrix} = \begin{pmatrix} N_A \\ N_R \end{pmatrix}$.

Finally, in the last panel, we observe how all the remaining separatrices of the saddles $S_{5,6,8,9}$ connect with some singular point at infinity.

In order to focus on the main aspects of the algorithm, along the paper we have concentrated on the generic cases; that is, no different singular points with the same energy level and no inflection points of F and G. For the sake of completeness, in Examples 3 and 4 we give instances of these non-generic situations.

Example 3. *The following example is special because there exist saddles points with the same level of energy, (see also panel (c) in Figure 14).*

$$\begin{cases} x' &= -y(y-1)(y-2), \\ y' &= x(x-2/5)(x-6/5)(x-2)(x^2+1). \end{cases} \tag{6}$$

In Fig. 14 we first present the graphs of F and G and then the distribution of their energy levels. Note that there are saddles with the same energy level, and so they create heteroclinic loops. Note that the singular points at infinity are nodes (applying Proposition 4 with m odd and n even). Moreover, since $a_n > 0$ and $b_n > 0$ we have that $\mathcal{Q} = \begin{pmatrix} A & \emptyset \\ R & \emptyset \end{pmatrix}$ and therefore $\begin{pmatrix} q_{inf}^+ \\ q_{inf}^- \end{pmatrix} = \begin{pmatrix} N_A \\ N_R \end{pmatrix}$. The global first portrait of system (6) is presented in the last panel of Figure 14.

Example 4. *To illustrate the algorithm in the presence of degenerate points, we provide the following example. Fig. 15 shows the process to obtain its global phase portrait.*

$$\begin{aligned} \dot{x} &= -(y-1)^2(y+5) \\ \dot{y} &= x(x+3)^2(x-6) \end{aligned} \tag{7}$$

Note that this phase portrait could have been obtained taking into account only the non-degenerate finite singular points (see Fig. 16) and then "adding by hand" the degenerate points.

4 Application: Bifurcation diagrams of families of Hamiltonian vector fields

A strong advantage of reducing the study of vector fields to the study of one-variable functions is that bifurcation diagrams for families of vector fields can be obtained from bifurcation diagrams

of functions. It is obvious that bifurcation values for F or G are the natural candidates to be the bifurcation values of the family of vector fields. However, in our case, since we have two one-variable functions involved, there will appear other bifurcation values related to the values of the functions at their critical points. Indeed, moving parameters it is possible to generate a new configuration (taking into account energy labelling) of singular points without crossing any bifurcation value of the one-variable function.

A simple (but not yet explored) family to illustrate this claim arises from considering F and G to be nonlinear monomials. In other words, we consider the family of Hamiltonian systems

$$\begin{cases} x' &= -y - a\, y^p, \\ y' &= x + b\, x^q, \end{cases} \tag{8}$$

with $a, b \in \mathbb{R}$, $p, q \in \mathbb{N} \setminus \{0, 1\}$ and $p \leq q$ (the case $p > q$ can be obtained from $p < q$ by switching the variables x and y). Thus, we have that

$$F(x) = \frac{x^2}{2} + b\frac{x^{q+1}}{q+1}, \qquad G(y) = \frac{y^2}{2} + a\frac{y^{p+1}}{p+1},$$

and the Hamiltonian function is

$$H(x, y) = \frac{x^2 + y^2}{2} + b\frac{x^{q+1}}{q+1} + a\frac{y^{p+1}}{p+1}. \tag{9}$$

Notice that $F'(x) = 0$ if and only if $x = 0$ or $x = (-1/b)^{1/(q-1)}$. Thus, if q is even, F will have 2 critical points, whereas if q is odd, F will have 1 critical point if $b > 0$ and 3 critical points if $b < 0$. An identical situation happens with the function G.

The values of the energy for the non-trivial critical points (when they exist) will be labelled as:

$$h_1 := F\left(\left(-\frac{1}{b}\right)^{\frac{1}{q-1}}\right), \quad h_2 := G\left(\left(-\frac{1}{a}\right)^{\frac{1}{p-1}}\right).$$

We will see below that the curve $h_1 = h_2$ plays an important role; in terms of parameters a and b it takes the implicit form:

$$(-1/a)^{2/(p-1)}\left(\frac{p-1}{p+1}\right) = (-1/b)^{2/(q-1)}\left(\frac{q-1}{q+1}\right), \tag{10}$$

whenever $(-1/a)^{1/(p-1)}$ and $(-1/b)^{1/(q-1)}$ are well defined.

We want to study the bifurcation scenarios with respect to the parameters a and b. According to other situations encountered along the paper, it is not surprising that the bifurcation diagrams depend strongly on the parities of p and q, and that we have to distinguish between $p < q$ and $p = q$. Therefore, we are going to consider the following six cases: (I) p odd, q even, $p < q$; (II) p even, q odd, $p < q$; (III) p even, q even, $p < q$; (IV) p odd, q odd, $p < q$; (V) $p = q$ odd; (VI) $p = q$ even.

For the sake of simplicity, we will concentrate all the general facts in the first case. In the remaining cases, we will also point out to specific issues and refer to the corresponding figure/s. The special nature of the functions F and G will also yield to some symmetries in the bifurcation diagram that will be specified for each case.

(I) p odd, q even, $p < q$.

With these parities, system (8) presents the symmetry $(-x, -y, -b) \longrightarrow (x,\ y,\ b)$, and therefore we restrict the study of systems (8) in the ab–plane with $b \geq 0$.

Fig. 17 covers all the possible qualitative graphs of F and G in this half plane, indicating the bifurcation curves for the phase portraits that we will encounter in Fig. 18.

For $a \geq 0$ and $b > 0$, in the finite plane there are two singular points: a centre $C = (0, 0)$ and a saddle $S = \left((-1/b)^{1/(q-1)},\ 0\right)$, which embraces the centre with two of its separatrices since, obviously, it is the neighbouring saddle with the closest energy level (C is of type C^+). Following the Table 1, the two singular points at infinity are nodes; the two free separatrices of S, then, join these nodes. See the phase portraits number 5 and 6 in Fig. 18.

For $a < 0$ and $b \neq 0$ there are six finite singular points:

- the three centres $C_\alpha = (0, 0)$, $C_{\beta\pm} = \left((-1/b)^{1/(q-1)}, \pm(-1/a)^{1/(p-1)}\right)$, and,
- the three saddles $S_{\alpha\pm} = \left(0,\ \pm(-1/a)^{1/(p-1)}\right)$ and $S_\beta = \left((-1/b)^{1/(q-1)},\ 0\right)$.

Observe that $H(S_{\alpha+}) = H(S_{\alpha-}) = h_2$ and $H(S_\beta) = h_1$. Thus, the curve $h_1 = h_2$ will separate different phase portraits and so, become a bifurcation curve. Hence, when $h_1 > h_2$ (see the phase portrait number 2 in Fig. 18), the saddles $S_{\alpha\pm}$ will be proximal (in energy) to the finite centre with lower energy C_α and will embrace them forming a heteroclinic connection, whereas S_β embraces the centres with highest energy, $C_{\beta\pm}$; when $h_1 = h_2$ (see the phase portrait number 3 in Fig. 18), heteroclinic connections among $S_{\alpha\pm}$ and S_β will arise; and, when $h_1 < h_2$ (see the phase portrait number 4 in Fig. 18), the saddle S_β will embrace the centre C_α, whereas the saddles $S_{\alpha\pm}$ will embrace the centres $C_{\beta\pm}$.

The case $a < 0$ and $b = 0$ (see the phase portrait number 1 in Fig. 18) yields to $p > q$ since the degree of F becomes two. Although we have ruled out in general this possibility, we will treat the case $b = 0$ for the sake of completeness. In the finite plane we have the centre $C = (0, 0)$ and the two saddles $S_{\alpha\pm} = \left(0,\ \pm(-1/a)^{1/(p-1)}\right)$. Since $H(S_{\alpha+}) = H(S_{\alpha+}) = h_2$, they form a heteroclinic connection embracing C (which is a centre of type C^+). The other separatrices form elliptic sectors at infinity. In this case, however, the points at infinity are located at the origin of the charts (U_1, ψ_1) and (V_1, ϕ_1), instead of (U_2, ψ_2) and (V_2, ϕ_2). This is due to the fact that the degree of G is higher than the degree of F, see Subsection 5.3 for more details.

The case $a > 0$ and $b = 0$ (see the phase portrait number 7 in Fig. 18), the only singular point is the centre at the origin, which is global. The only nuance is that there are two hyperbolic sectors at infinity.

The case $a = b = 0$ appears in all the cases and represents the linear centre.

(II) p even, q odd, $p < q$.

In this case, system (8) presents the symmetry

$$(-x, -y, -a) \longrightarrow (x,\ y,\ a),$$

and therefore we restrict its study to the ab–plane with $a \geq 0$. Working in a similar way than in Case I we obtain the bifurcation diagrams displayed in Fig. 19. The main difference with Case I is that the singular points are arranged "orthogonally" and so, since the singular

points at infinity are placed at the same place, they interact forming different singular points at infinity (elliptic+hyperbolic instead of nodes), in agreement with Table 1.

(III) p even, q even, $p < q$.

In this case, system (8) presents the symmetries

$$(-x,-y,-a,-b) \longrightarrow (x,\ y,\ a,\ b),\ (-x,-t,-b) \longrightarrow (x,\ t,\ b),\ (-y,-t,-a) \longrightarrow (y,\ t,\ a),$$

and therefore we can restrict the study of systems (8) to the first quadrant of the ab-plane $(a, b \geq 0)$.

For any pair (a, b) with $a\,b > 0$, there are four finite singular points: two centres, $(C_\alpha = (0,0)$ and $C_\beta = \left((-1/b)^{1/(q-1)},\ (-1/a)^{1/(p-1)}\right)$, and two saddles, $S_b = \left((-1/b)^{1/(q-1)}, 0\right)$, $S_a = \left(0,\ (-1/a)^{1/(p-1)}\right)$. Depending on the sign of $h_1 - h_2$ we obtain the phase portraits number 2, 3 and 4 in Fig. 20. The main difference is the organization of the separatrices: C_α is always embraced by the lowest energy level saddle, and C_β by the highest energy level saddle. If $h_1 < h_2$ (resp., $>$), S_b is the lowest saddle (resp., highest).

When $a = 0$ or $b = 0$, then only two singular points exist: one centre and one saddle which embraces the centre. The arrangement of the finite singular points is on the x-axis with two separatrices going to the origin of the charts (U_2, ψ_2), (V_2, ϕ_2) if $a = 0$ (see phase portrait number 1 in Fig. 20), whereas finite singular points are arranged along the y-axis with two separatrices going to the origin of the charts (U_1, ψ_1), (V_1, ϕ_1) if $b = 0$ (see phase portrait number 5 in Fig. 20).

In the following cases, we will omit the bifurcations of the graphs of F and G and explain directly the bifurcations of the vector fields.

(IV) p odd, q odd, $p < q$.

In this case, there are no symmetries that could simplify the bifurcation diagram. The fact that p and q are both odd, leads to the following situation:

- in the first ab-quadrant, there is a unique finite singular, which is a centre, see phase portraits number 5, 6 and 7 in Fig. 21;
- in the second and fourth ab-quadrants, one of the two functions has 3 critical points, so the system has 3 finite singular points (two saddles and one centre), ones arranged along the x-axis and the other along the y-axis. Heteroclinic connections embrace the centre, and the other separatrices form elliptic sectors at infinity, see phase portraits number 4 and 8 in Fig. 21;
- the case $a < 0$, $b = 0$ is similar to $a < 0$, $b > 0$, but the elliptic sectors are follow different directions towards infinity, as it happens in previous cases, see phase portrait number 3 in Fig. 21;
- in the third ab-quadrant, both F and G have 3 critical points, so we have 9 finite singular points (5 saddles and 4 centres). As in previous cases, the connections will depend on the sign of $h_1 - h_2$. See phase portraits number 9, 1 and 2 in Fig. 21;

(V) $p = q$ odd. This case is very similar to Case (IV). In the finite part, everything is the same, but in the infinity, the elliptic sectors (except the case $a = 0$ or $b = 0$ which remain identical) split into two nodes, according to (14). This affects only the phase portraits 4 and 8 in Fig. 21. As an example, in Fig. 22 how phase portrait 8 in Fig. 21 is transformed when $p = q$.

(VI) $p = q$ even. This case is identical to Case (III). The only difference could happen at infinity, as for Cases (IV) and (V), but in this case, due to the parity, the singular points at infinity persist when equating the degrees.

We have only taken one example because it is rich enough, but the algorithms presented in this paper allow to easily treat parametric families of Hamiltonian systems with separate variables.

5 Technical results

This section is devoted to the proofs of the results used in the previous sections to build up the algorithm. We start with those concerning singular points in Subsection 5.1. In Subsection 5.2, we give technical lemmas to unveil the local phase portrait in the planar cells whose vertices are the finite singular points. These lemmas are then useful to prove the results about singular points at infinity in Subsection 5.3, and also the global organisation of separatrices in Subsection 5.4.

5.1 Finite singular points

We give the proof of Proposition 1 (topological classification of finite singular points).

Proof of Proposition 1. We will give a unified proof that includes both hyperbolic and non-hyperbolic singular points (linear centres, cusps and double hyperbolic sectors) from the geometry of the level curves of the Hamiltonian function around them.

Let us suppose, without loss of generality, that F has a maximum at x_0 and G has a minimum at y_0. According to statement (a), we must prove that (x_0, y_0) is a saddle point.

Let $h_0 = H(x_0, y_0) = F(x_0) + G(y_0)$. Since x_0 is a maximum of F and y_0 is a minimum of G, given a small enough punctured neighbourhood of x_0, U_{x_0}, for any $x \in U_{x_0}$, there exist two values $y_1(x)$, $y_2(x)$ close to y_0 such that $F(x)+G(y_i(x)) = h_0$, for $i = 1, 2$, satisfying $y_1(x_0) = y_2(x_0) = y_0$. Thus, (x_0, y_0) is topologically equivalent to a saddle point. Observe that each of the four quadrants centred at (x_0, y_0) contains one and only one separatrix, thus defining four hyperbolic sectors, see also Fig. 8.

In the chosen case, the values of the Hamiltonian function on the left and right sectors will be smaller than h_0 whereas on the upper and lower sectors will be higher.

It is straightforward to obtain the topological classification of all the other types of singular points mentioned in the statement using the same type of reasoning. Let us mention only some specific differences.

In the case of two maxima (resp., two minima), it is clear that no separatrices arrive at (x_0, y_0) and there exists a neighbourhood of (x_0, y_0) filled up by closed orbits whose energy levels decrease (resp., increase) with the distance to (x_0, y_0).

In the case of F having an inflection point at x_0 and G having a maximum (minimum) at y_0,

it is easy to see that, if F is increasing in a neighbourhood of x_0, then only the two right (left) separatrices appear. If F is decreasing in a neighbourhood of x_0, the situation is reversed.

□

5.2 Dynamics in rectangular cells

As it was already introduced in Section 2.3, finite singular points are the corners of a tiling of the Poincaré disk. According to the values of the energy function on the corners of a cell, it is possible to know the relative positions of orbits in each cell. In this section we give two technical lemmas which will be useful to prove the results on singular points at infinity and organisation of separatrices. For the sake of the clearness, we will only consider saddles or centres; cuspidal points and singular points with two hyperbolic sectors can be ruled out from the discussion following next remark.

Remark 12. *Let us suppose that all the zeroes of F' and G' have odd multiplicity; thus, applying Proposition 1, all the singular points of (2) are either saddles or centres.*

Denote by x_i, with $i = 1, \dots, r$, the zeroes of F' and define now $\tilde{F}(x)$ such that: (a) x_i, for all $i = 1, \dots, r$, keep the same multiplicity; (b) for some $k \in \{1, \dots, r\}$, there exists $\tilde{x} \in (x_k, x_{k+1})$ being a zero of $\tilde{F}'$ of even multiplicity. Then,

1. *$\tilde{x}$ is an inflection point of $\tilde{F}$;*
2. *the phase portrait of the Hamiltonian vector field given by $H(x, y) = F(x) + G(y)$ is topologically equivalent to that of $\tilde{H}(x, y) = \tilde{F}(x) + G(y)$ except for the presence of cuspidal points at $(\tilde{x}, y_j)$, for $j = 1, \dots, s$.*

The same argument could be applied to G. Similarly, the study of systems with singular points being the union of two hyperbolic sectors can be reduced to "equivalent" systems having all the zeroes of F' and G' with odd multiplicity.

In other words, the remark states that singular points (x^*, y^*) so that x^* or y^* are critical points of F or G with even multiplicity can be added artificially to the phase portrait after applying the algorithm.

Notice that, in the generic conditions stated in Remark 12, the corners of a rectangular cell are two saddles (situated in opposite corners) and two centres.

We define $\alpha_i := F(x_i) - F(x_{i-1})$, for $i = 2, \dots, r$, and $\beta_j := G(y_j) - G(y_{j-1})$, for $j = 2, \dots, s$. Additionally, we define $\alpha_1 = (-1)^n \, sgn(a_n) \cdot \infty$, $\alpha_{r+1} = sgn(a_n)\infty$, $\beta_1 = (-1)^m \, sgn(b_m) \, \infty$ and $\beta_{s+1} = sgn(b_m)\infty$, where n and m are the degrees of F' and G', respectively; in particular, $r \leq n$ and $s \leq m$.

Next result gives the behaviour of the separatrices in each of the rectangular cells R_{ij}, see also Fig. 23.

Lemma 13. *Consider a rectangular cell R_{ij}, with $1 \leq i < r$ and $2 \leq j < s$. Then,*

1. *If $\alpha_{i+1} > 0$ and $\beta_{j+1} > 0$, then the phase portrait in the rectangular cell R_{ij} is one of the following:*

   (a) *As in panel A of Fig. 23 if $\alpha_{i+1} > \beta_{j+1}$.*

   (b) *As in panel B of Fig. 23 if $\alpha_{i+1} = \beta_{j+1}$.*

   (c) *As in panel C of Fig. 23 if $\alpha_{i+1} < \beta_{j+1}$.*

2. *If $\alpha_{i+1} > 0$ and $\beta_{j+1} < 0$, we have Fig. 23.A rotated 90º clockwise if $|\alpha_{i+1}| < |\beta_{j+1}|$, Fig. 23.B rotated 90º clockwise if $|\alpha_{i+1}| = |\beta_{j+1}|$ or Fig. 23.C rotated 90º clockwise if $|\alpha_{i+1}| > |\beta_{j+1}|$.*

3. *If $\alpha_{i+1} < 0$ and $\beta_{j+1} < 0$, we have Fig. 23.A rotated 180º if $|\alpha_{i+1}| > |\beta_{j+1}|$, Fig. 23.B rotated 180º if $|\alpha_{i+1}| = |\beta_{j+1}|$ or Fig. 23.C rotated 180º if $|\alpha_{i+1}| < |\beta_{j+1}|$.*

4. *If $\alpha_{i+1} < 0$ and $\beta_{j+1} > 0$, we have Fig. 23.A rotated 270º clockwise if $|\alpha_{i+1}| < |\beta_{j+1}|$, Fig. 23.B rotated 270º clockwise if $|\alpha_{i+1}| = |\beta_{j+1}|$ or Fig. 23.C rotated 270º clockwise if $|\alpha_{i+1}| > |\beta_{j+1}|$.*

Proof of Lemma 13. We first prove item (1). First of all, observe that the vector field (2) satisfies $\dot{x} < 0$ and $\dot{y} > 0$ on R_{ij}.

Since $\alpha_{i+1} > 0$ and $\beta_{j+1} > 0$, the singular points on the border of the cell R_{ij} are of the following types: $\{C_{i,j}, S_{i,j+1}, C_{i+1,j+1}, S_{i+1,j}\}$, where the first entry refers to the down-left corner of R_{ij}, and the others follow a clockwise order, see Fig. A. In particular the energy values of the four singular points satisfy $H(S_{i,j+1}) = H(C_{i,j}) + \beta_{j+1}$, $H(S_{i+1,j}) = H(C_{i,j}) + \alpha_{i+1}$ and $H(C_{i+1,j+1}) = H(C_{i,j}) + \alpha_{i+1} + \beta_{j+1}$.

In the case that $\alpha_{i+1} > \beta_{j+1}$, we have that $H(C_{i,j}) < H(S_{i,j+1}) < H(S_{i+1,j}) < H(C_{i+1,j+1})$. Thus, the upper-left separatrix of $S_{i+1,j}$ must exit the cell R_{ij} through the edge between $S_{i,j+1}$ and $C_{i+1,j+1}$ since all the other edges of R_{ij} are banned either because of the direction of the vector field or because the energy level $H(S_{i+1,j})$ is not contained in the set of energy levels of that edge. The other three separatrices of $S_{i+1,j}$ belong to a three different neighbouring cells ($R_{i+1,j}$, $R_{i,j-1}$, $R_{i+1,j-1}$).

Analogously, the down-right separatrix of $S_{i,j+1}$ intersects the border of R_{ij} through the edge between $C_{i,j}$ and $S_{i+1,j}$.

Having controlled the behaviour of the two separatrices, the dynamics in R_{ij} is completely determined since, moreover, any orbit cannot intersect the same edge more than once.

When $\alpha_{i+1} = \beta_{j+1}$, note that the two separatrices coincide and so, the phase portrait in R_{ij} is the one given in Fig. 23.B.

When $\alpha_{i+1} < \beta_{j+1}$, using similar arguments, it is straightforward to see that the separatrix of $S_{i+1,j}$ intersects the edge between $C_{i,j}$ and $S_{i,j+1}$, whereas the separatrix of $S_{i,j+1}$ intersects the edge between $C_{i+1,j+1}$ and $S_{i+1,j}$, see Fig. 23.C.

The same mechanisms can be applied to the hypotheses of statements (2, 3, 4). Observe that, for instance, the hypothesis of statement (2), $\alpha_{i+1} > 0$ and $\beta_{j+1} < 0$ is equivalent to consider the case of statement (1) with $\tilde{\alpha}_{i+1} > 0$, $\tilde{\beta}_{j+1} > 0$, and then apply the change $\alpha_{i+1} = \tilde{\beta}_{j+1}$, $\beta_{j+1} = -\tilde{\alpha}_{i+1}$.

This is equivalent to rotate clockwise 90^o the corresponding phase portrait obtained for $\tilde{\alpha}_{i+1}$ and $\tilde{\beta}_{j+1}$ from statement (1). For instance, the subcase $\tilde{\alpha}_{i+1} > \tilde{\beta}_{j+1}$ will become $|\alpha_{i+1}| < |\beta_{j+1}|$, and similarly for the other two subcases $|\alpha_{i+1}| = |\beta_{j+1}|$ and $|\alpha_{i+1}| > |\beta_{j+1}|$.

Statements (3) and (4) follow in a similar way. □

Next lemma describes the dynamics on the unbounded cells. Note that the information we give is purely topological since we do not pay attention to the direction of the vector field. In any case, it is trivial to establish this direction.

Lemma 14. *The following statements hold:*

(a) Let Q be a corner cell for system (2) whose border is formed by a finite singular point p and the two half-lines L_x and L_y intersecting at p.

(a.1) If p is a centre, then all the orbits in Q connect L_x with L_y.

(a.2) If p is a saddle, then the separatrix of p lying on Q escapes to (comes from) infinity, as well as any orbit intersecting L_x or L_y.

(b) Let Q be a semi-rectangular cell for system (2) whose border is formed by the segment joining two finite singular points p (centre) and q (saddle) and two half-lines L and L' satisfying $p \in L$ and $q \in L'$. Then, the separatrix of p lying on Q crosses L'.

Proof of Lemma 14. Let us first prove statement (a), devoted to corner cells. Following the notation given in Definition 3, we consider the upper-right cell Q^{++}. The other corner have symmetric behaviours and so we do not lose generality. The direction of the vector field on Q^{++} depends on the signs of the derivatives of F and G on the intervals $I_\infty := (x_r, +\infty)$ and $J_\infty := (y_s, +\infty)$, respectively. Observe that:

(a.1) if $F' > 0$ on I_∞ and $G' > 0$ on J_∞, then (x_r, y_s) is a centre point and the direction of the vector field on Q^{++} is determined by $\dot{x} < 0$ and $\dot{y} > 0$. Let us consider then a point $z := (x, y_s) \in L_x$ with $x > x_r$. Notice that the orbit $\varphi(t; z)$ such that $\varphi(t; z) = z$ has negative slope for for $t > 0$ and, for $t = 0$, we have that $\dot{x} = 0$ and $\dot{y} > 0$. So, for any $t > 0$, $\varphi(t; z) \in Q^{++}$. Since x_r and y_s are the highest extrema of F and G, the second derivatives of F and G cannot vanish on Q^{++} and so, the curvature $((F''(x)G'(y)^2 + G''(y)F'(x)^2)/(F'(x)^2 + G'(y)^2)^{3/2}\Big|_{\varphi(t;z)})$ of $\varphi(t; z)$ is positive on Q^{++}. Finally, considering any point $z_1 = \varphi(t_1; z)$, with $t_1 > 0$, the tangent line to $\varphi(t; z)$ at $t = t_1$ together with L_x and L_y form a positively invariant region (we call it Ω) for the flow φ. Since $Int(\Omega)$ cannot contain any singular point inside (recall that p, on the boundary, is a centre) and $\dot{y} > 0$ on Ω, then $\varphi(t; z)$ must reach L_y in finite time, as we wanted to prove. Thus, any orbit starting on the horizontal half-line L_x will intersect L_y at some $t > 0$.

If $F' < 0$ and $G' < 0$, only the direction changes ($\dot{x} > 0$ and $\dot{y} < 0$) and so, any orbit starting on the vertical half-line L_y will intersect L_x at some $t > 0$.

(a.2) if $F' < 0$ on I_∞ and $G' > 0$ on J_∞, then $p := (x_r, y_s)$ is a saddle point and the direction vector field on Q^{++} is determined by $\dot{x} < 0$ and $\dot{y} < 0$. Thus, the rr-separatrix of p cannot escape from Q^{++} and tends for $t \to -\infty$ to a singular point at infinity. If $F' > 0$ and $G' < 0$,

only the direction changes ($\dot{x} > 0$ and $\dot{y} > 0$) and so, the rr-separatrix of p tends to a singular point at infinity for $t \to +\infty$.

Statement (b) is devoted to semi-rectangular cells, delimited by two corner points p and q, their common segment $\overline{pq}$ and the half-lines called L (from p to infinity) and L' (from q to infinity). Without loss of generality, we can assume that p is a centre and q is a saddle point. From the proof statement (a.1) we know that one of the separatrices of q crosses Q until it reaches the half-line L (at some point that we call p'). On the other hand, from the proof of statement (a.2), all the orbits from segment $\overline{pq}$ also intersect L, between p' and p. Finally, by the same arguments, all the other orbits (that is, those starting on L') must intersect L. □

5.3 Singular points at infinity

We give the proofs of Lemma 2 (number of singular points at the infinity of the Poincaré sphere) and Proposition 4 (topological classification).

Proof of Lemma 2. We assume that the vector field (2) has been compactified using the Poincaré compactification, see Section 2.3 to recall the notation.

As we will appreciate in the following cases, the charts of the Poincaré compactification will contain singular points depending on the sign and parity of $n - m$.

Case 1: $n > m$.

In the (U_1, ψ_1) chart the vector field takes the form

$$\left\{ \begin{array}{rcl} \dot{z_1} & = & z_2^n \left(z_1\, G'(\frac{z_1}{z_2}) + F'(\frac{1}{z_2}) \right) \\ & = & a_n + a_{n-1} z_2 + \cdots + a_1 z_2^{n-1} + b_m z_1^{m+1} z_2^{n-m} + \cdots + b_1 z_1^2 z_2^{n-1}, \\ \dot{z_2} & = & z_2^{n+1}\, G'(\frac{z_1}{z_2}) = z_2^{n-m+1}(b_m z_1^m + b_{m-1} z_1^{m-1} z_2 + \cdots + b_1 z_1 z_2^{m-1}). \end{array} \right. \tag{11}$$

We note that there are no singular points on $\{z_2 = 0\}$ since $a_n \neq 0$.

In the (U_2, ψ_2) chart the vector field can be written as

$$\left\{ \begin{array}{rcl} \dot{z_1} & = & -z_2^n \left(G'(\frac{1}{z_2}) + z_1\, F'(\frac{z_1}{z_2}) \right) \\ & = & -b_m z_2^{n-m} - \cdots - b_1 z_2^{n-1} - a_n {z_1}^{n+1} - \cdots - a_1 {z_1}^2 z_2^{n-1}, \\ \dot{z_2} & = & -z_2^{n+1}\, F'(\frac{z_1}{z_2}) = -a_n {z_1}^n z_2 - \cdots - a_1 z_1 z_2^n, \end{array} \right. \tag{12}$$

which has a unique singular point, $z_1 = z_2 = 0$, on $\{z_2 = 0\}$.

Case 2: $n = m$

On the (U_1, ψ_1) chart, the vector field becomes

$$\left\{ \begin{array}{rcl} \dot{z_1} & = & (a_n + b_n\, {z_1}^{n+1}) + (a_{n-1} + b_{n-1}\, {z_1}^n) z_2 + \ldots + (a_1 + b_1\, {z_1}^2) z_2^{n-1}, \\ \dot{z_2} & = & z_2 (b_n\, {z_1}^n + \ldots + b_1\, z_1). \end{array} \right. \tag{13}$$

We note that singular points at infinity are given by

$$z_1{}^{n+1} = -\frac{a_n}{b_n}. \tag{14}$$

On the (U_2, ψ_2) chart the vector field writes as

$$\begin{cases} \dot{z_1} &= -b_n - b_{n-1}\, z_2 - \ldots - b_1\, z_2^{n-1} - a_n\, z_1{}^{n+1} - a_{n-1}\, z_1{}^n\, z_2 \\ & \quad - \ldots - a_1\, z_1{}^2\, z_2^{n-1}, \\ \dot{z_2} &= -z_2\,(a_n\, z_1{}^n + \ldots + a_1\, z_1\, z_2^{n-1}), \end{cases} \tag{15}$$

and the singular points at infinity are given by $z_1{}^{n+1} = -\dfrac{b_n}{a_n}$.

Then, when n is odd and $\frac{b_n}{a_n} < 0$, we have 2 singular points on all the charts: (U_1, ψ_1), (V_1, ϕ_1), (U_2, ψ_2) and (V_2, ϕ_2). However, the 4 singular points on (U_1, ψ_1) and (V_1, ϕ_1) coincide (on the Poincaré sphere) with the 4 singular points on (U_2, ψ_2) and (V_2, ϕ_2) since $z_1^{n+1} = -a_n/b_n$ on U_1 and $z_2^{n+1} = -b_n/a_n$ on U_2 represent the same directions at infinity on the Poincaré sphere. When n is even, the situation is repeated but with only 1 singular point per chart; thus, we have 2 singular points at infinity.

We recall that, after an appropriate change of variables, the case $n < m$ is equivalent to the case $n > m$. □

Once the number and position of singular points is established, we prove the results that classify them topologically.

Proof of Proposition 4. In fact, from Lemma 14 we know that:

- an orbit can reach (either for $t \to +\infty$ or for $t \to -\infty$) the point at infinity only through a corner cell; that, is there are no orbits reaching infinity through a semi-rectangular cell.
- to reach infinity through a corner cell $Q^{\sigma\sigma'}$, σ, $\sigma' \in \{+, -\}$, the sign of the vector field has to be $\pm(\sigma, \sigma')$.

We assume now that $n > m$; for $n = m$, the conclusions are the same, except that the singular points at infinity are not located at the same places. In the case of two critical points, the compactified phase portraits will not change topologically. In the case of four critical points, it may happen, as the only topological difference, that the elliptic sectors split into two mutually connected nodal sectors, see for instance Figure 25.

In the proof of Lemma 14 we have analyzed the direction of the vector field on $Q^{\sigma\sigma'}$ in terms of the derivative of F on I_∞ and the derivative of G on J_∞. More precisely, we can repeat the arguments in terms of the degree and the sign of the leading coefficients of F and G.

Let us suppose, for instance, that n is even and m is odd and let us focus only on those corner cells with a saddle on its vertex (by Lemma 14 (a.1), centres are less related to the stability of singular points at infinity). We have that:

1. if $a_n > 0$, $b_m > 0$, the singular point q^-_{inf} is repelling on Q^{--} and q^+_{inf} is attracting on Q^{-+}.
2. if $a_n < 0$, $b_m > 0$, the singular point q^-_{inf} is attracting on Q^{+-} and q^+_{inf} is repelling on Q^{++}.
3. if $a_n > 0$, $b_m < 0$, the singular point q^-_{inf} is repelling on Q^{+-} and q^+_{inf} is attracting on Q^{++}.
4. if $a_n < 0$, $b_m < 0$, the singular point q^-_{inf} is attracting on Q^{--} and q^+_{inf} is repelling on Q^{-+}.

Then, using the notation already introduced in the statement of the proposition and Table 1, it can be summarized in Table 2.

n	m	a_n	b_m	Q^{--}	Q^{+-}	q^-_{inf}	Q^{-+}	Q^{++}	q^+_{inf}
even	odd	$+$	$+$	R	$\emptyset$	N_R	A	$\emptyset$	N_A
even	odd	$+$	$-$	$\emptyset$	R	N_R	$\emptyset$	A	N_A
even	odd	$-$	$+$	A	$\emptyset$	N_A	R	$\emptyset$	N_R
even	odd	$-$	$-$	$\emptyset$	A	N_A	$\emptyset$	R	N_R

Table 2: Attracting or repelling sectors of singular points at infinity as a function of degrees and signs of F and G.

From Table 2 we obtain the matrices $\mathcal{Q}$ in the left-down corner of Table 1 straightforwardly. From $\mathcal{Q}$, we get the classification of the singular points just observing that a pattern $(A/R \quad \emptyset)$ in a row of $\mathcal{Q}$ implies that the corresponding point is an attracting/repelling node with the entry direction on the left corner cell; the pattern $(A/R \quad R/A)$ implies that the corresponding point has an elliptic sector; and, finally, the pattern $(\emptyset \quad \emptyset)$ implies that the corresponding point presents a hyperbolic sector.

□

Just as a question of coherence with other possible reasonings that have not been used here, observe that Proposition 6 matches with the results that one would obtain by applying index theory. Indeed, the degrees n, m plus the sign of the coefficients a_n and b_m give all the information about the index of the vector field at the finite singular points $\mathbb{R}^2$; then, using the Poincaré-Hopf Theorem we can extract information about the indices of singular points at infinity as next remark shows.

Remark 15. *We denote by $i_{X_H}(\mathbb{R}^2)$ the sum of indices (see [?] for a definition of index) of all the finite singular points and by $i_{\overline{X_H}}(\{X_3 = 0\})$ the sum of indices of the singular points lying on the equator of the Poincaré sphere. Since $i_{X_H}(\mathbb{R}^2)$ is the sum of indices on the chart (U_3, ψ_3) and the Euler characteristics of the sphere is two, we have that*

$$2\, i_{X_H}(\mathbb{R}^2) + i_{\overline{X_H}}(\{X_3 = 0\}) = 2. \tag{16}$$

Then,

1. *If n is even, $i_{X_H}(\mathbb{R}^2) = 0$ and $i_{\overline{X_H}}(\{X_3 = 0\}) = 2$ (see Figure 6(d)).*
2. *If n is odd and m is even, then $i_{X_H}(\mathbb{R}^2) = 0$ and $i_{\overline{X_H}}(\{X_3 = 0\}) = 2$ (see Figure 6(a)).*

3. If n is odd and m is odd, then either

(a) $i_{X_H}(\mathbb{R}^2) = -2$ and $i_{\overline{X_H}}(\{X_3 = 0\}) = 4$ (see Figure 6(b)); or,

(b) $i_{X_H}(\mathbb{R}^2) = 2$ and $i_{\overline{X_H}}(\{X_3 = 0\}) = 0$ (see Figure 6(c)).

5.4 Organisation of separatrices

Lemmas 13 and 14 give a first level description of the behaviour of the orbits in the "tiled" plane. The results of Section 2.4 rely on these properties. Thus, from these lemmas, we are able to prove properties of other structures appearing in the phase portrait like the organisation of bounded and unbounded separatrices which were stated in Proposition 6, Proposition 8 and Proposition 11.

Proof of Proposition 6. It follows from the proof of Proposition 4 after observing the relationship between the properties of the saddles (see Definition 5) and the direction of the vector field at the corner cells. Indeed, we have (with the notation used in Table 2):

- $\mathcal{F}_l$ (resp., f_l) $\Rightarrow \left(\begin{array}{c|c} \dot{y} > (<)0 & * \\ \hline \dot{y} > (<)0 & * \end{array}\right)$; $\mathcal{F}_r$ (resp., f_r) $\Rightarrow \left(\begin{array}{c|c} * & \dot{y} < (>)0 \\ \hline * & \dot{y} < (>)0 \end{array}\right)$;
- $\mathcal{G}_l$ (resp., g_l) $\Rightarrow \left(\begin{array}{c|c} * & * \\ \hline \dot{x} < (>)0 & \dot{x} < (>)0 \end{array}\right)$; $\mathcal{G}_r$ (resp., g_r) $\Rightarrow \left(\begin{array}{c|c} \dot{x} > (<)0 & \dot{x} > (<)0 \\ \hline * & * \end{array}\right)$.

Consequently:

$$(\mathcal{F}_l, g_r) \text{ (resp., } (f_l, \mathcal{G}_r)) \Rightarrow \left(\begin{array}{c|c} A\ (R) & * \\ \hline * & * \end{array}\right); \qquad (f_r, \mathcal{G}_r) \text{ (resp., } (\mathcal{F}_r, g_r)) \Rightarrow \left(\begin{array}{c|c} * & A\ (R) \\ \hline * & * \end{array}\right).$$

$$(f_l, \mathcal{G}_l) \text{ (resp., } (\mathcal{F}_l, g_l)) \Rightarrow \left(\begin{array}{c|c} * & * \\ \hline A\ (R) & * \end{array}\right); \qquad (\mathcal{F}_r, g_l) \text{ (resp., } (f_r, \mathcal{G}_l)) \Rightarrow \left(\begin{array}{c|c} * & * \\ \hline * & A\ (R) \end{array}\right);$$

Consider, for instance, a saddle point $S^* := (x_{i^*+1}, y_{j^*+1})$ of type $(f_l, \mathcal{G}_l)$ (in Fig. 26, for instance, $i^* = 2 = j^*$).

If $j^* = 0$ and $i^* > 0$ (similarly if $i^* = 0$ and $j^* > 0$), then S^* is a corner of a semi-rectangular cell that can be expressed as $R_{i^*,0} := (x_{i^*}, x_{i^*+1}) \times (-\infty, y_1)$. Since S^* is of type $\mathcal{G}_l$, then $G' > 0$ on $(-\infty, y_1)$ and so, $\dot{x} < 0$ on the semi-rectangular cells $R_{i,0}$ such that $i < i^*$. Then, applying Lemma 14 (a), the *ll*-separatrix of S^* crosses all these semi-rectangular cells until it reaches R_{00} (the left-down corner cell called also Q^{--}). By Lemma 14 (b), then, the *ll*-separatrix of tends to q^-_{inf}.

If $i^* = j^* = 0$, then S^* is the corner of the corner cell R_{00} and the last part of the previous argument suffices.

In the case that $i^* \neq 0$ and $j^* \neq 0$, we first observe that all the points $H(x, y_{j^*+1}) > H(S^*)$ for all $x < x_{i^*+1}$, and $H(x_{i^*+1}, y) < H(S^*)$ for all $y < y_{j^*+1}$. This observation implies that the *ll*-separatrix of S^* is confined to the region $(-\infty, x_{i^*+1}) \times (-\infty, y_{j^*+1})$ (see Fig. 26). Then,

applying Lemma 13 successively, one can conclude the the ll-separatrix will end into some of the semi-rectangular cells R_{ij}, with $i = 0$ and $j < j*$ or with $j = 0$ and $i < i*$. In both cases, the arguments given above apply again and the conclusion follows. The path to reach R_{00} will depend on the values of H on the saddles (x_i, y_j), with $i \leq i*$ and $j \leq j*$ and cannot be determined knowing only that $S^* \in f_l \cap \mathcal{G}_l$.

□

Proof of Proposition 8. The proofs of statements (a) and (b) are similar. Without loss of generality, then, we assume to have a singular point $C = (x_i, y_j)$ of type C^+. We also assume to be in the most general case: $1 < i < r$ and $1 < j < s$. The other cases differ only in the number of possible neighbouring saddles.

In this case, it is straightforward to see that (in the hat (in the notation of Lemma 13) $\alpha_i < 0$, $\alpha_{i+1} > 0$, $\beta_j < 0$ and $\beta_{j+1} > 0$. Let us suppose that the neighbouring saddle point S^* whose energy level satisfies $H(S^*) = \min_{S \in \mathcal{N}_C} \{H(S) : H(S) > H(C)\}$ is $S^* = (x_{i-1}, y_j)$ (a non-restrictive hypothesis). Applying Lemma 13 to the rectangular cells $R_{i-1,j-1}$ and $R_{i-1,j}$, we can deduce that the separatrices of S^* proximal to C intersect the segments $\overline{(x_i, y_j)(x_i, y_{j+1})}$ and $\overline{(x_i, y_{j-1})(x_i, y_j)}$. Applying again Lemma 13, now to the rectangular cells $R_{i,j-1}$ and $R_{i,j}$, we conclude that these two separatrices must intersect the segment $\overline{(x_i, y_j)(x_{i+1}, y_j)}$ and, since H is monotone on this segment, form a loop.

To prove statement (c), we assume again to be in the most general situation: $S = (x_i, y_j)$ with $1 < i < r$ and $1 < j < s$. We want to prove that S cannot be the proximal saddle of two different centers of different type (C^+ and C^-).

We then consider the grid Γ formed by S and the other 8 singular points that surround it (4 neighbouring centres and 4 saddles, in the corners of this grid). Recall that either x_i is a local minimum of F and y_j is a local maximum of G or x_i is a local maximum of F and y_j is a local minimum of G. Let us assume the latter case, in which the centers satisfy $H(x_{i-1}, y_j), H(x_{i+1}, y_j) < H(S)$ and $H(x_i, y_{j-1}), H(x_i, y_{j+1}) > H(S)$; or, equivalently, $\alpha_{i+1} < 0$, $\beta_j < 0$ and $\alpha_i > 0$, $\beta_{j+1} > 0$. If we denote by $C^+_{-1} := (x_{i-1}, y_j)$ and $C^+_1 := (x_{i+1}, y_j)$ the centers of type C^+, and by $C^-_{-1} := (x_i, y_{j-1})$ and $C^-_1 := (x_i, y_{j+1})$ the centers of type C^-, then we have that $H(C^+_{i_1}) \leq H(C^+_{i_2}) < H(S) < H(C^-_{j_2}) \leq H(C^-_{j_1})$, considering an adequate reordering of indices such that $\{i_1, i_2\} = \{j_1, j_2\} = \{-1, 1\}$; this reordering depends on the ordering of the values $|\alpha_i|$, $|\alpha_{i+1}|$,$|\beta_j|$ and $|\beta_{j+1}|$.

Let us take now the saddle $\overline{S} := (x_{i+i_2}, y_{j+j_2})$. Observe that $H(\overline{S}) = H(C^+_{i_2}) + H(C^-_{j_2}) - H(S)$ and so, $H(\overline{S}) \in \{H(C^+_{i_2}), H(C^-_{j_2})\}$ since $H(C^-_{j_2}) - H(S) > 0$ and $H(C^+_{i_2}) - H(S) < 0$. If $H(\overline{S}) = H(S)$, then there would be a heteroclinic connection between these two saddles and so, the separatrices of S could not embrace two centers simultaneously. If $H(\overline{S}) \neq H(S)$, then S cannot satisfy simultaneously $H(S) = \min_{S' \in \mathcal{N}_{C^+_{i_2}}} \{H(S') : H(S') > H(C^+_{i_2})\}$ and $H(S) = \max_{S' \in \mathcal{N}_{C^-_{j_2}}} \{H(S') : H(S') < H(C^-_{j_2})\}$. According to statements (a) and (b), then, S can only embrace one type of centre. □

The arguments used to prove Proposition 8 work for Proposition 11 as well, just considering the extended graphics as centre points.

Software tools

All the global phase portraits have been obtained with the free software P4, see [**?**] or http://mat.uab.cat/%7Eartes/p4/p4.htm.

Acknowledgments

The authors are grateful to Armengol Gasull for suggestive discussions and bear in mind the first steps of this work together with Elena Manresa.

References

[AVK87] A. A. Andronov, A. A. Vitt, and S. È. Khaĭkin. *Theory of oscillators*. Dover Publications Inc., New York, 1987. Translated from the Russian by F. Immirzi, Reprint of the 1966 translation.

[CGM00] Anna Cima, Armengol Gasull, and Francesc Mañosas. Period function for a class of Hamiltonian systems. *J. Differential Equations*, 168(1):180–199, 2000. Special issue in celebration of Jack K. Hale's 70th birthday, Part 1 (Atlanta, GA/Lisbon, 1998).

[CJ89] Carmen Chicone and Marc Jacobs. Bifurcation of critical periods for plane vector fields. *Trans. Amer. Math. Soc.*, 312(2):433–486, 1989.

[CL07a] Laurent Cairó and Jaume Llibre. Phase portraits of cubic polynomial vector fields of Lotka-Volterra type having a rational first integral of degree 2. *J. Phys. A*, 40(24):6329–6348, 2007.

[CL07b] Laurent Cairó and Jaume Llibre. Phase portraits of quadratic polynomial vector fields having a rational first integral of degree 2. *Nonlinear Anal.*, 67(2):327–348, 2007.

[Con87] Roberto Conti. Centers of quadratic systems. *Ricerche Mat.*, 36(suppl.):117–126, 1987.

[CR91] J. Candy and W. Rozmus. A symplectic integration algorithm for separable Hamiltonian functions. *J. Comput. Phys.*, 92(1):230–256, 1991.

[DLA06] Freddy Dumortier, Jaume Llibre, and Joan C. Artés. *Qualitative theory of planar differential systems*. Universitext. Springer-Verlag, Berlin, 2006.

[FGG04] Emilio Freire, Armengol Gasull, and Antoni Guillamon. First derivative of the period function with applications. *J. Differential Equations*, 204(1):139–162, 2004.

[GGM00] Armengol Gasull, Antoni Guillamon, and Victor Mañosa. Phase portrait of Hamiltonian systems with homogeneous nonlinearities. *Nonlinear Anal.*, 42(4, Ser. A: Theory Methods):679–707, 2000.

[Gol51] Herbert Goldstein. *Classical Mechanics*. Addison-Wesley Press, Inc., Cambridge, Mass., 1951.

[Ily04] Yulij Ilyashenko. Selected topics in differential equations with real and complex time. In *Normal forms, bifurcations and finiteness problems in differential equations*, volume 137 of *NATO Sci. Ser. II Math. Phys. Chem.*, pages 317–354. Kluwer Acad. Publ., Dordrecht, 2004.

[Jon95] Christopher K. R. T. Jones. Geometric singular perturbation theory. In *Dynamical systems (Montecatini Terme, 1994)*, volume 1609 of *Lecture Notes in Math.*, pages 44–118. Springer, Berlin, 1995.

[KLML96] Jung-Hoon Kim, Seung-Woo Lee, Hans Maassen, and Hai-Woong Lee. Relativistic oscillator of constant period. *Phys. Rev. A*, 53(5):2991–2997, May 1996.

[LA07] Dina Shona Laila and Alessandro Astolfi. Direct discrete-time design for sampled-data Hamiltonian control systems. In *Lagrangian and Hamiltonian methods for nonlinear control 2006*, volume 366 of *Lecture Notes in Control and Inform. Sci.*, pages 87–98. Springer, Berlin, 2007.

[Lou64] W. S. Loud. Behavior of the period of solutions of certain plane autonomous systems near centers. *Contributions to Differential Equations*, 3:21–36, 1964.

[LR04] Benedict Leimkuhler and Sebastian Reich. *Simulating Hamiltonian dynamics*, volume 14 of *Cambridge Monographs on Applied and Computational Mathematics*. Cambridge University Press, Cambridge, 2004.

[MST02] Raymond G. McLenaghan, Roman G. Smirnov, and Dennis The. Group invariant classification of separable Hamiltonian systems in the Euclidean plane and the O(4)-symmetric Yang-Mills theories of Yatsun. *J. Math. Phys.*, 43(3):1422–1440, 2002.

[Per91] Lawrence Perko. *Differential equations and dynamical systems*, volume 7 of *Texts in Applied Mathematics*. Springer-Verlag, New York, 1991.

[SS02] Mark Sofroniou and Giulia Spaletta. Symplectic methods for separable Hamiltonian systems. In *Computational science—ICCS 2002, Part III (Amsterdam)*, volume 2331 of *Lecture Notes in Comput. Sci.*, pages 506–515. Springer, Berlin, 2002.

[Sto49] Henry Stommel. Trajectories of small bodies sinking slowly through convection cells. *J. Marine Research*, 8:24–29, 1949.

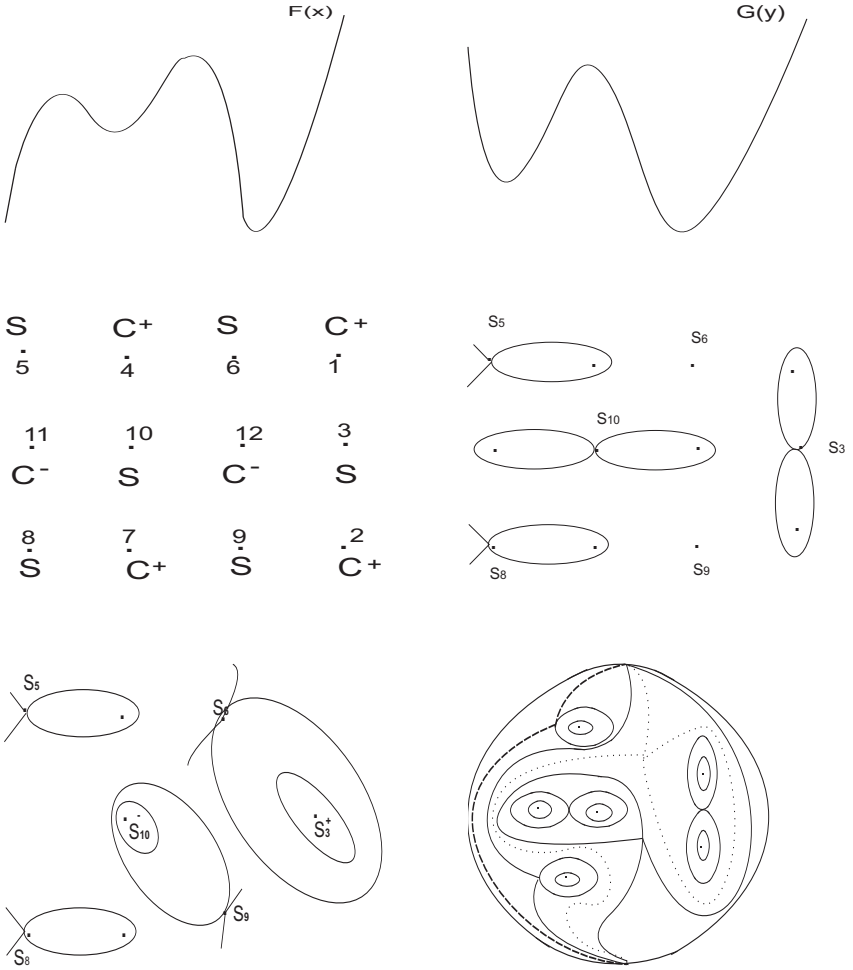

Figure 13: The upper panels show the qualitative plots of functions F and G of system (5). The left panel in the centre row contains the classification, labelling and energy ordering of the finite singular points. The other three panels represent different steps in the application of the algorithm: first, neighbouring saddles embracing the centres (central row); second (lowest row, left), the neighbouring saddles embracing the extended graphics S_3^+ and S_{10}^+; third, and last, the global phase portrait (drawn qualitatively for the sake of clarity). Note that the singular points at infinity are nodes, according to Table 1.

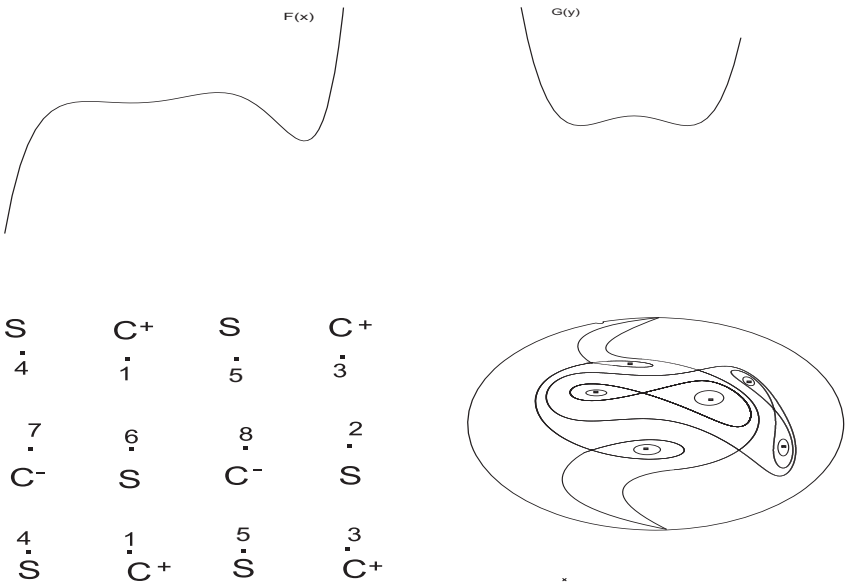

Figure 14: Graphs of F and G, finite singular points and global phase portrait of system (6). Notice the heteroclinic connections between saddles of the same energy level.

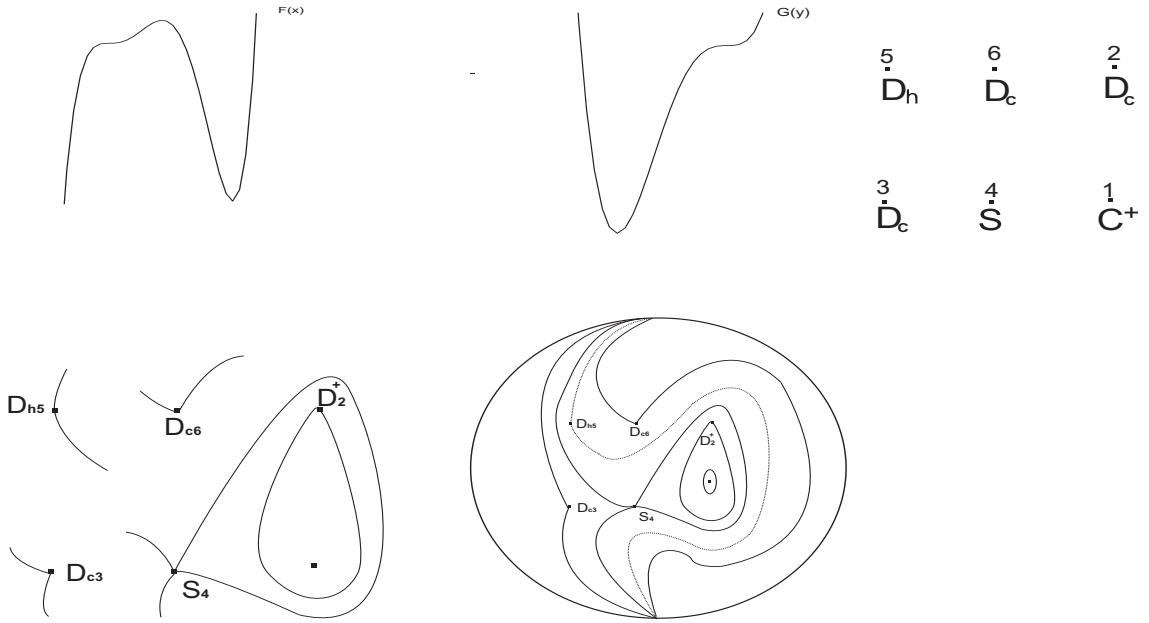

Figure 15: Graphs of F and G, finite singular points and global phase portrait of system (7). Notice the presence of degenerate points.

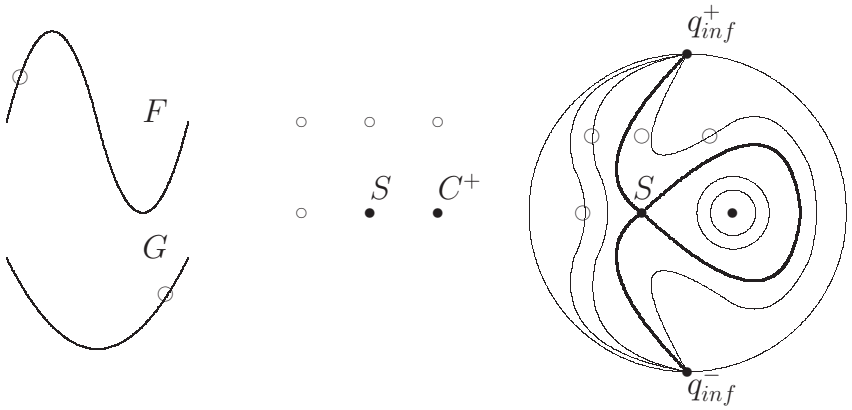

Figure 16: The process to obtain the global phase portrait of system (7) ignoring the degenerate points. Empty circles indicate either the location of inflection points of F and G or degenerate points. Pictures are just a qualitative description.

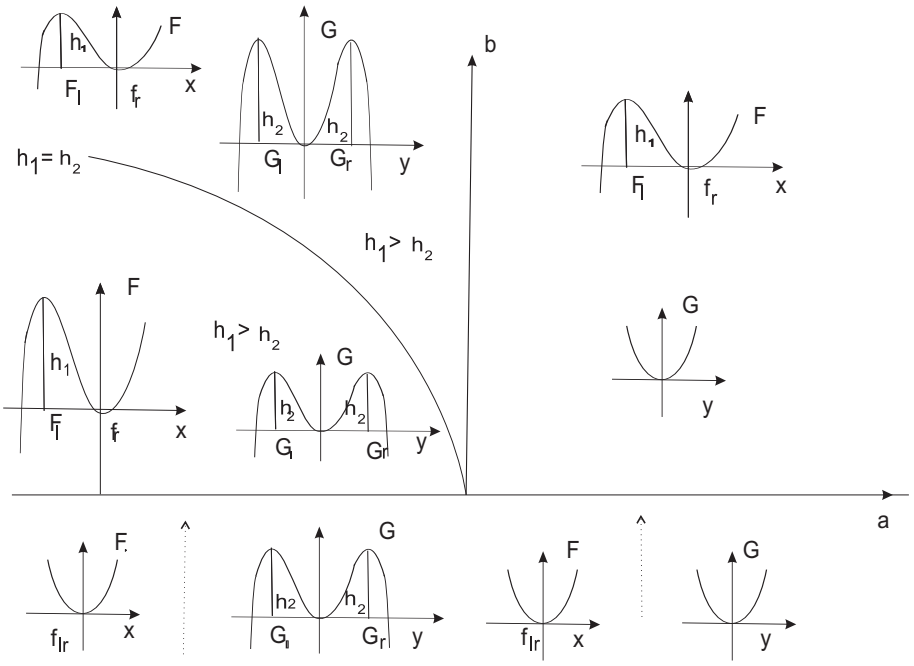

Figure 17: Case I: Bifurcation diagrams of the graphs of F and G for $(\mathbf{p}, \mathbf{q})$ =(odd, even), taking into account the curve $h_1 = h_2$.

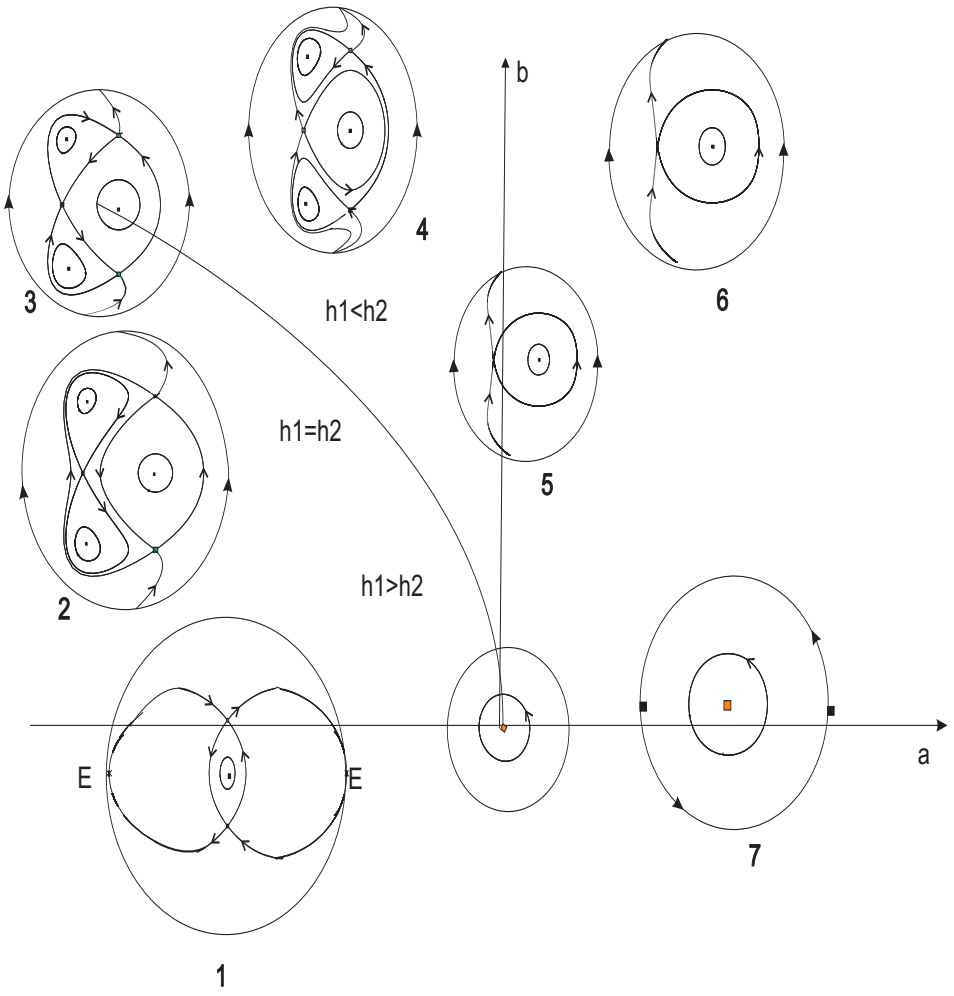

Figure 18: Case I: bifurcation diagrams of (8) corresponding to p odd and q even.

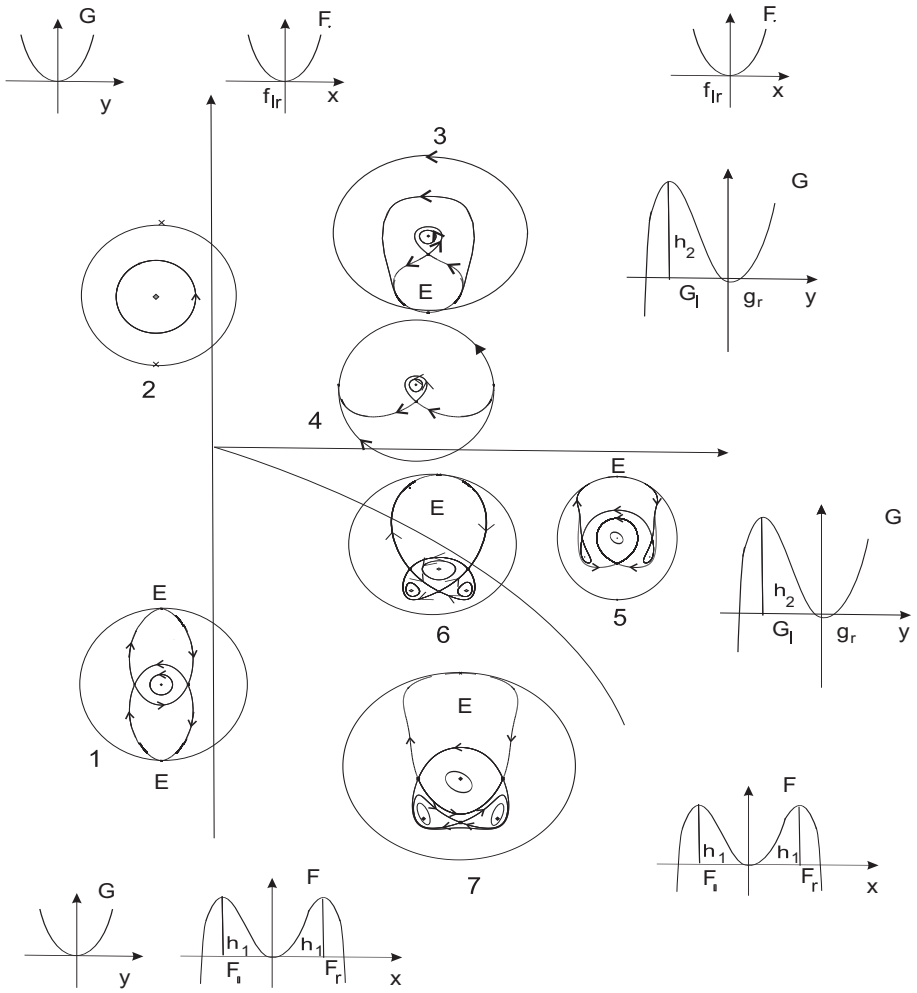

Figure 19: Case II: bifurcation diagrams of (8) corresponding to p even and q odd.

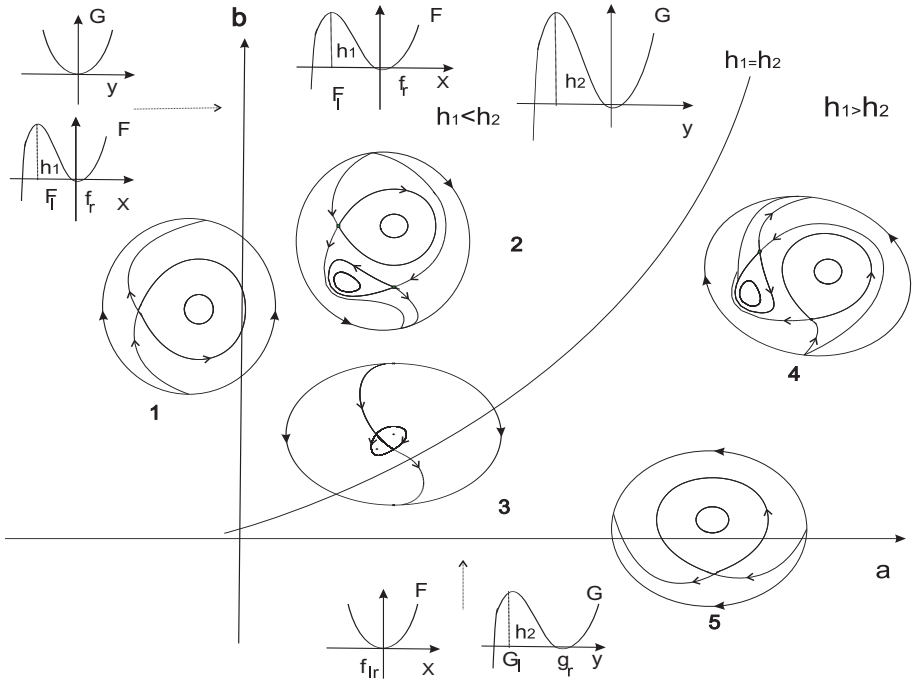

Figure 20: Case III: Bifurcation diagrams of (8) corresponding to p even and q even, along with the changes in the functions F and G.

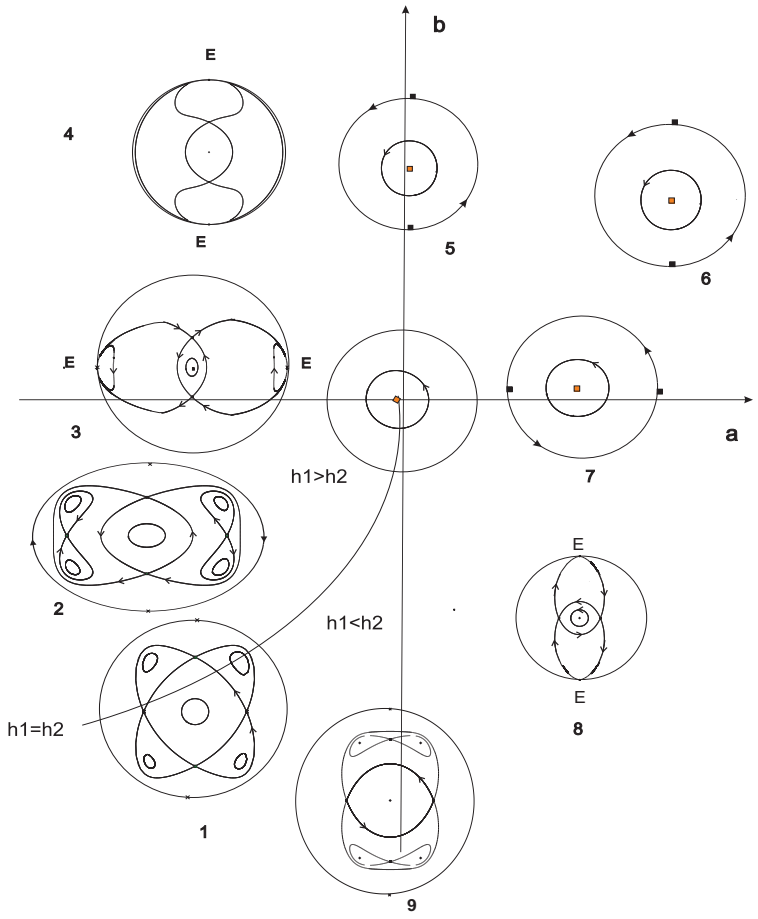

Figure 21: Case IV: bifurcation diagrams of (8) corresponding to p odd and q odd.

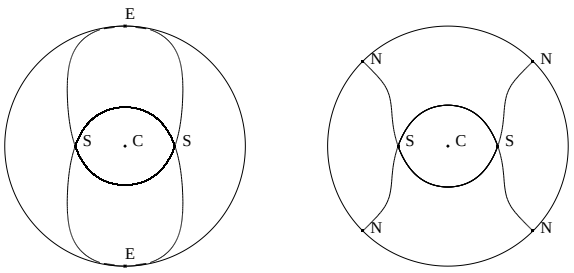

Figure 22: Case V: Change in the phase portrait 8 in Fig. 21 (left) when $p = q$ (right).

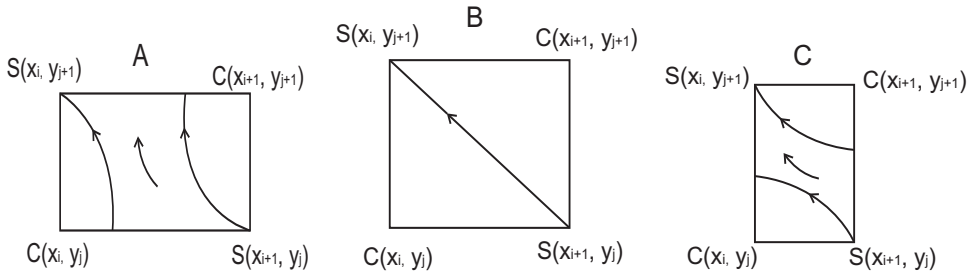

Figure 23: Possible phase portraits (modulo rotations) in a rectangular cell R_{ij}.

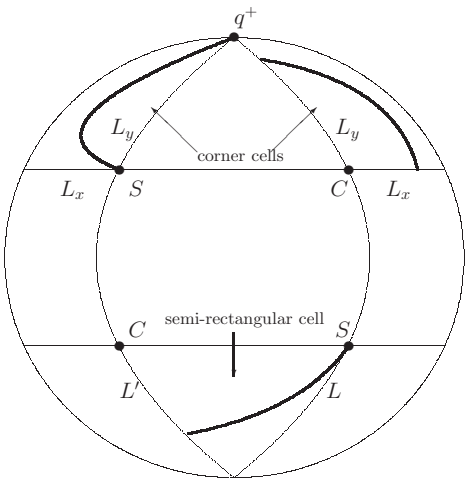

Figure 24: Phase portraits in the semi-rectangular and corner cells. The three possible types of orbits are shown schematically. As in Lemma 14, L is the generic labelling for half-lines joining finite and infinite singular points.

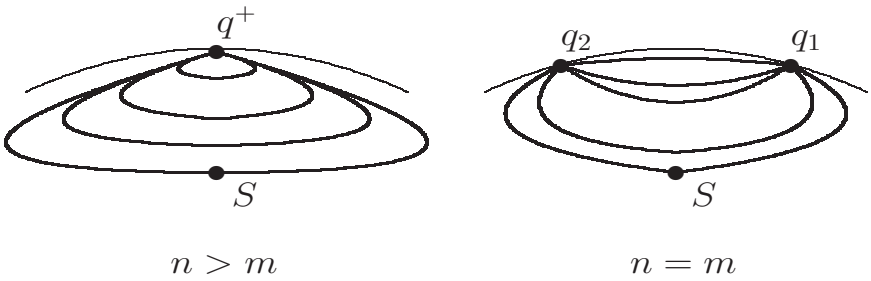

Figure 25: Schematic representation of how a singular point at infinity (q^+_{inf}) having an elliptic sector for $n > m$ splits into two point (q_1, q_2) with nodal sectors for $n = m$.

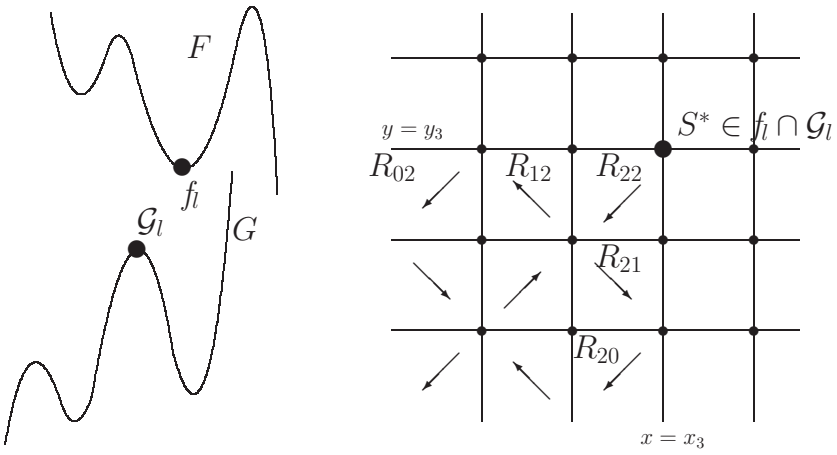

Figure 26: Standard configuration with a saddle point of types f_l ang $\mathcal{G}_l$, to illustrate the proof of Proposition 6. Here, $S^* = (x_3, y_3)$.